COLLÈGE DE FRANCE
1530

UNIVERSITÉ GRENOBLE ALPES

Chaire de Physique de la Matière Condensée

Matériaux et dispositifs à fortes corrélations électroniques

II.2 Contrôle des fonctionnalités des oxydes: flims minces, heterostructures

Antoine Georges

Cycle 2014-2015
18 mai 2015 – II.2

CONTROL: Traditional and Novel routes

Bandwidth	Pressure Size of rare-earth Distortion Tolerance factor 3d,4d,5d metal	Strained thin films and heterostructures Light/non-linear phononics
Crystal field, Orbital degeneracy	Size of rare-earth Distortion Tolerance factor	- Same -
Filling of shell	Chemistry	Ionic liquids Gating
Doping	$Sr,Ca^{2+} \rightarrow La, R^{3+}$	
Interaction strength	3d,4d,5d metal	Tunable dielectric gating ? Light ?
Charge-Transfer	Change apical oxygen distance Change ligand: O→ S, Se…	Light ?

Two routes to control

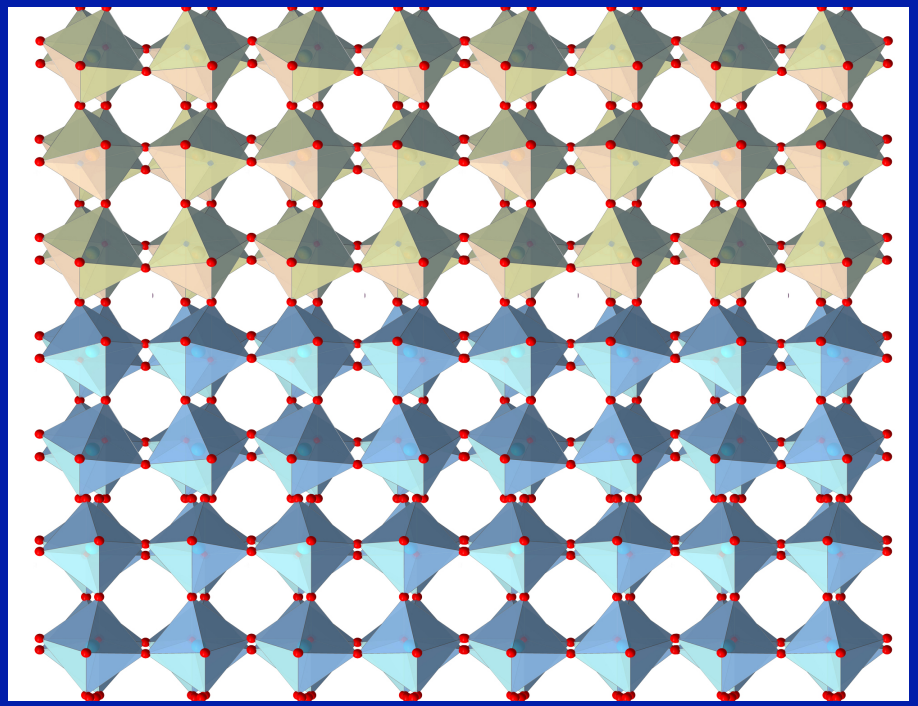

Artificial Materials:
Strained films and
Heterostructures
"Oxytronics/Mottronics"

Selective control with LIGHT

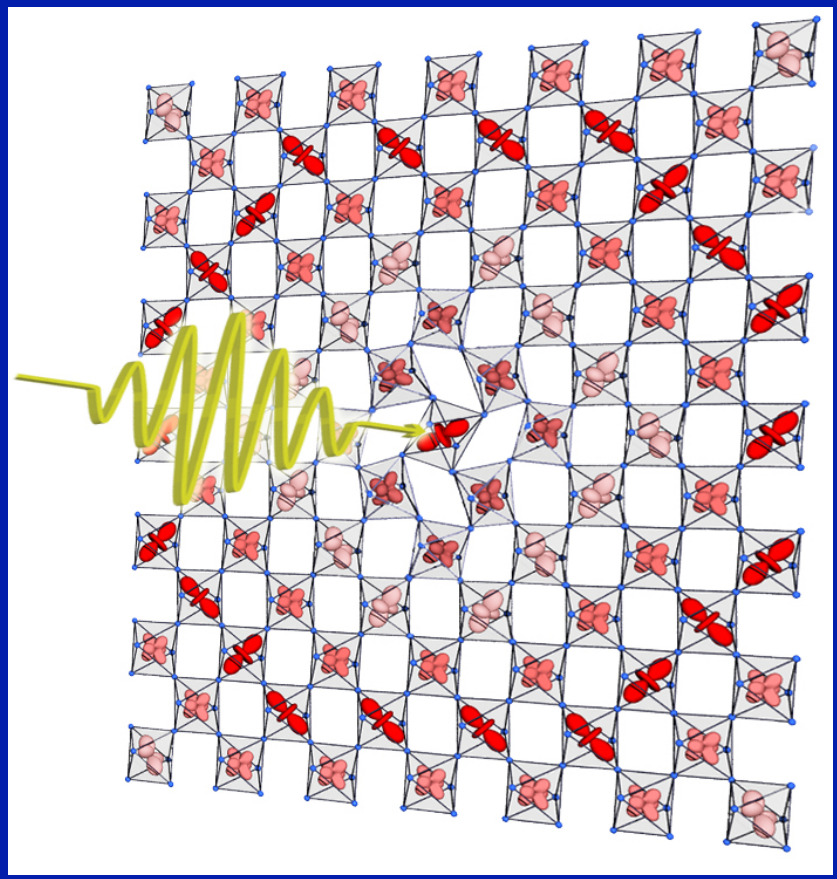

Can we teach correlated quantum materials to do what we want them to: SELECTIVE CONTROL of structure (and electronic structure) ?

"Frontiers in Quantum Materials Control"
ERC-Synergy project QMAC
A.Cavalleri, A.G., D.Jaksch, J.M. Triscone

http://www.mpsd.mpg.de/48916/Q-MAC-start

1. Progress in materials elaboration technique

- Sputtering
- Pulsed Laser Deposition
- Molecular Beam Epitaxy

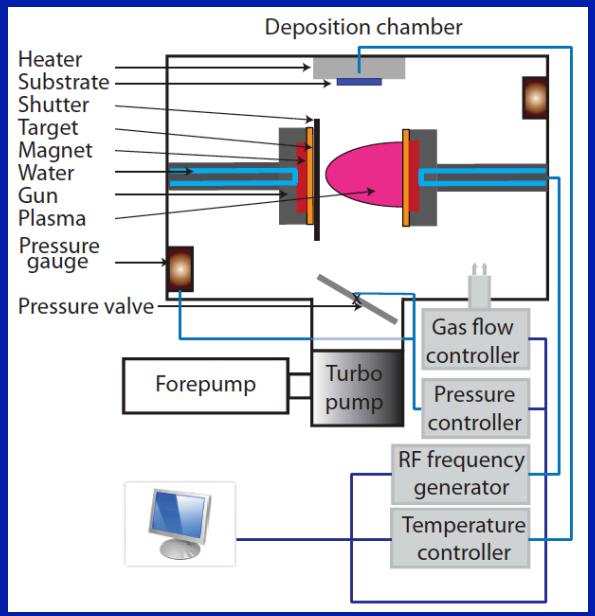

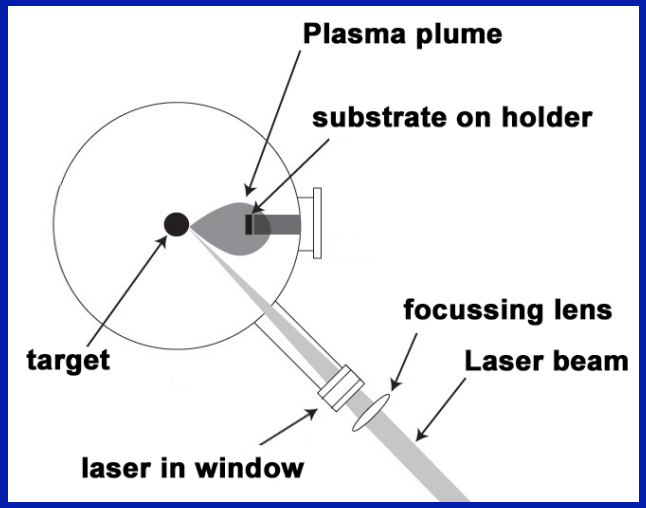

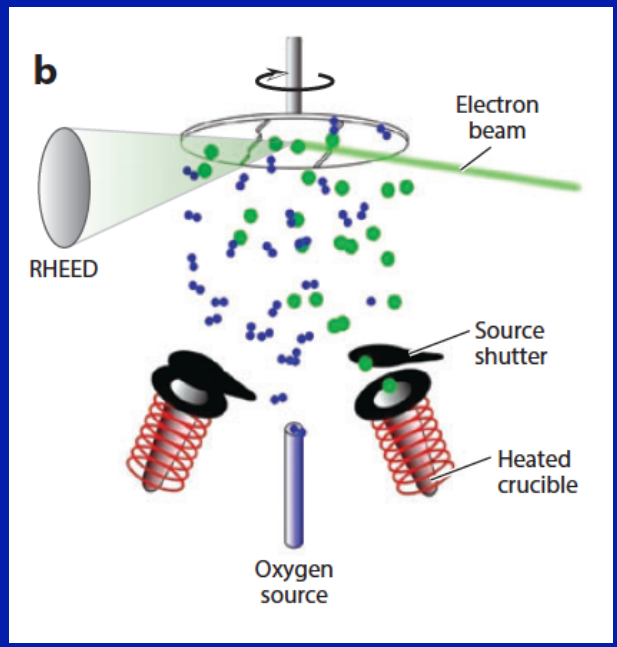

Molecular Beam Epitaxy (MBE)

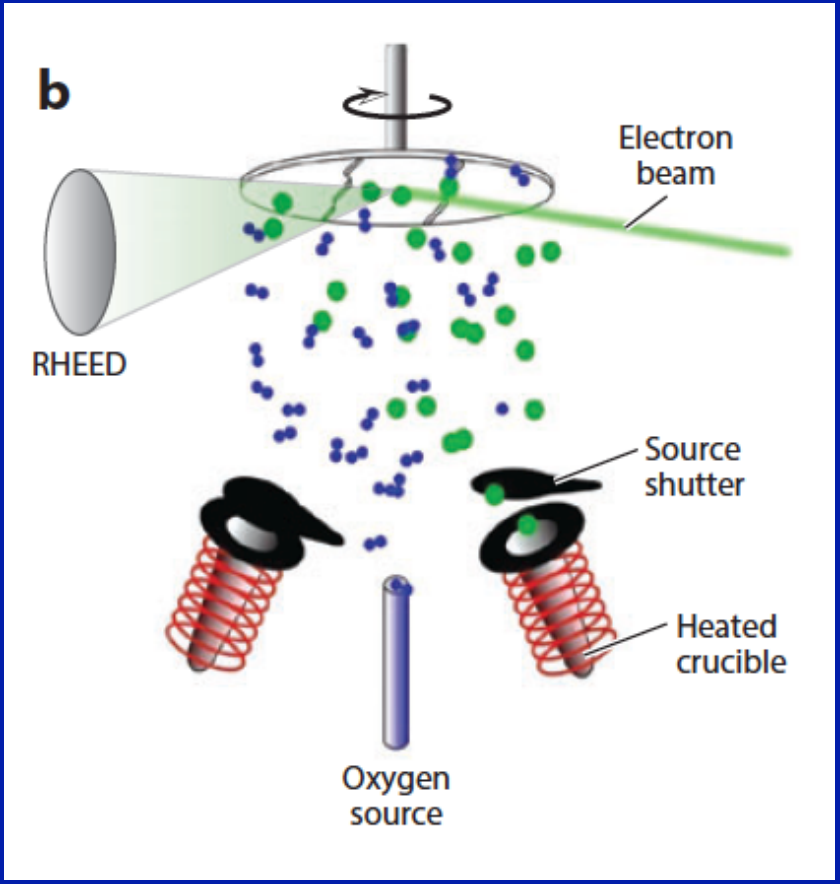

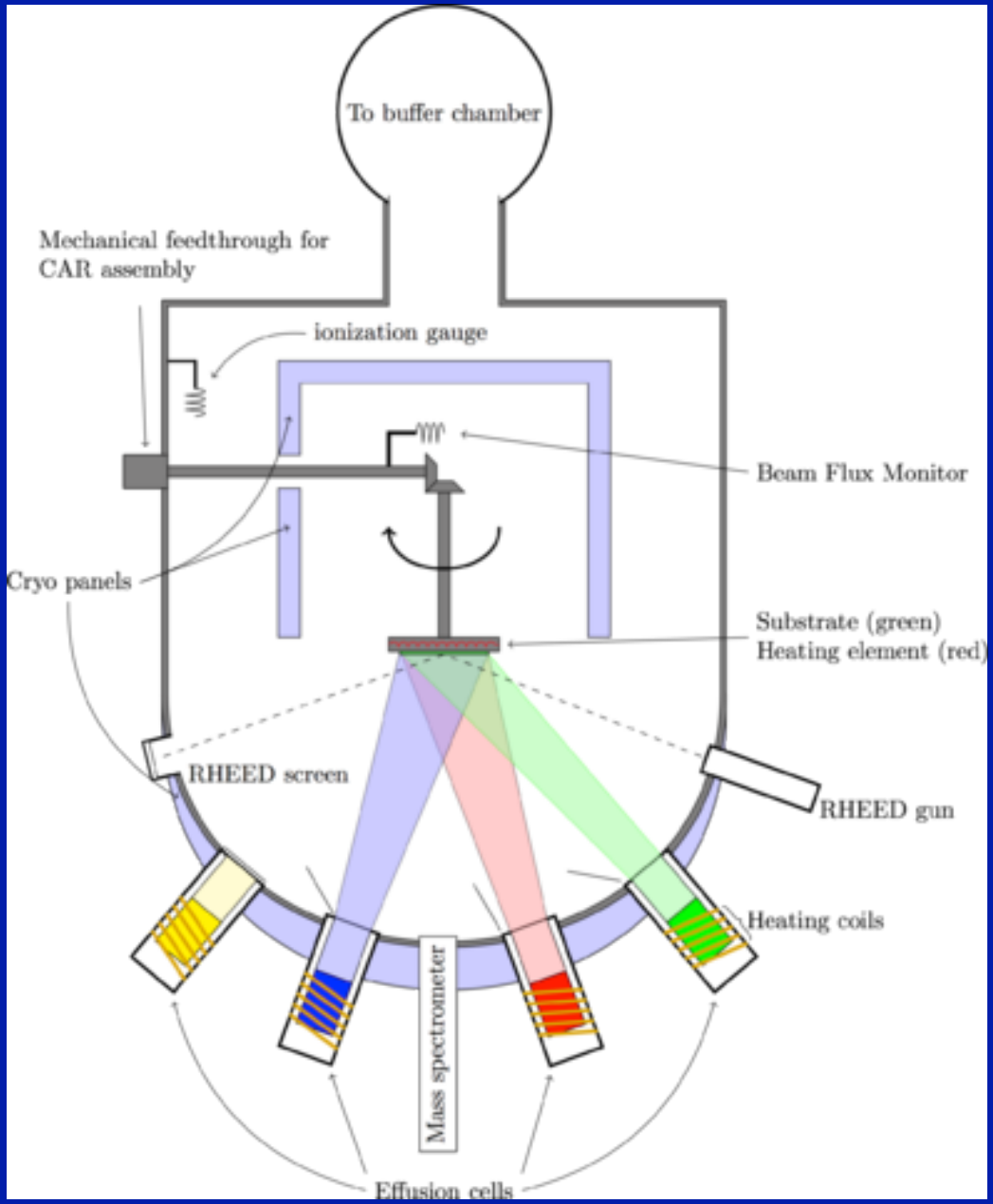

Oxide heterostructures by MBE

Artificial charge-modulation in atomic-scale perovskite titanate superlattices

Nature 419, 378 (2002)

A. Ohtomo, D. A. Muller, J. L. Grazul & H. Y. Hwang

Bell Laboratories, Lucent Technologies, Murray Hill, New Jersey 07974, USA

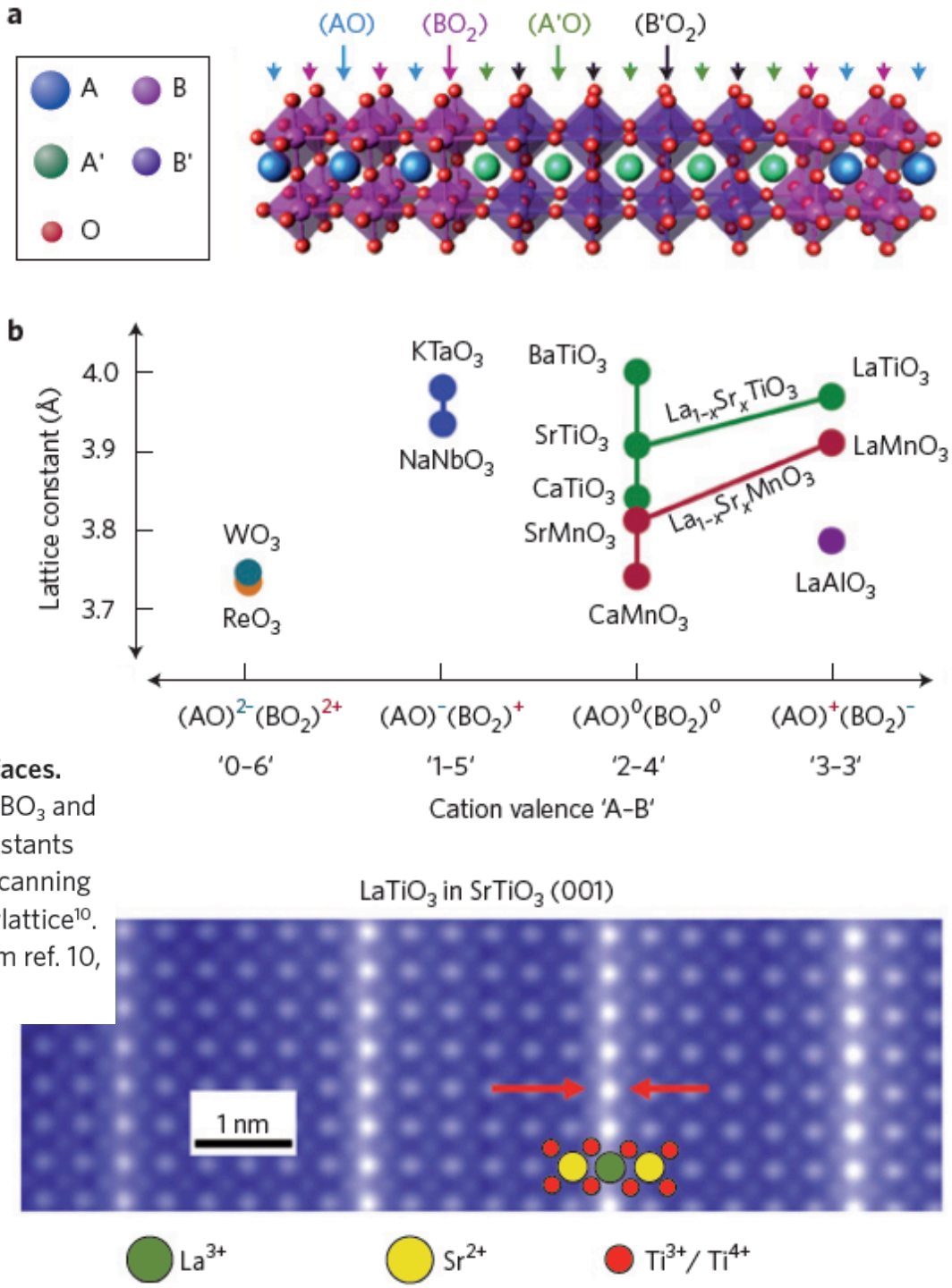

Figure 3 | Atomic and charge structure of pervoskite heterointerfaces. **a**, Schematic of ideal heterointerfaces between two perovskites, ABO_3 and $A'B'O_3$ stacked in the [001] direction. **b**, Representative lattice constants for various perovskites as a function of their charge sequence. **c**, Scanning transmission electron microscopy image of a $LaTiO_3/SrTiO_3$ superlattice[10]. The red arrows show the lanthanum layer. Panel **c**, reproduced from ref. 10, © 2002 NPG.

Hwang et al.
Nature Mat
11 103 (2012)

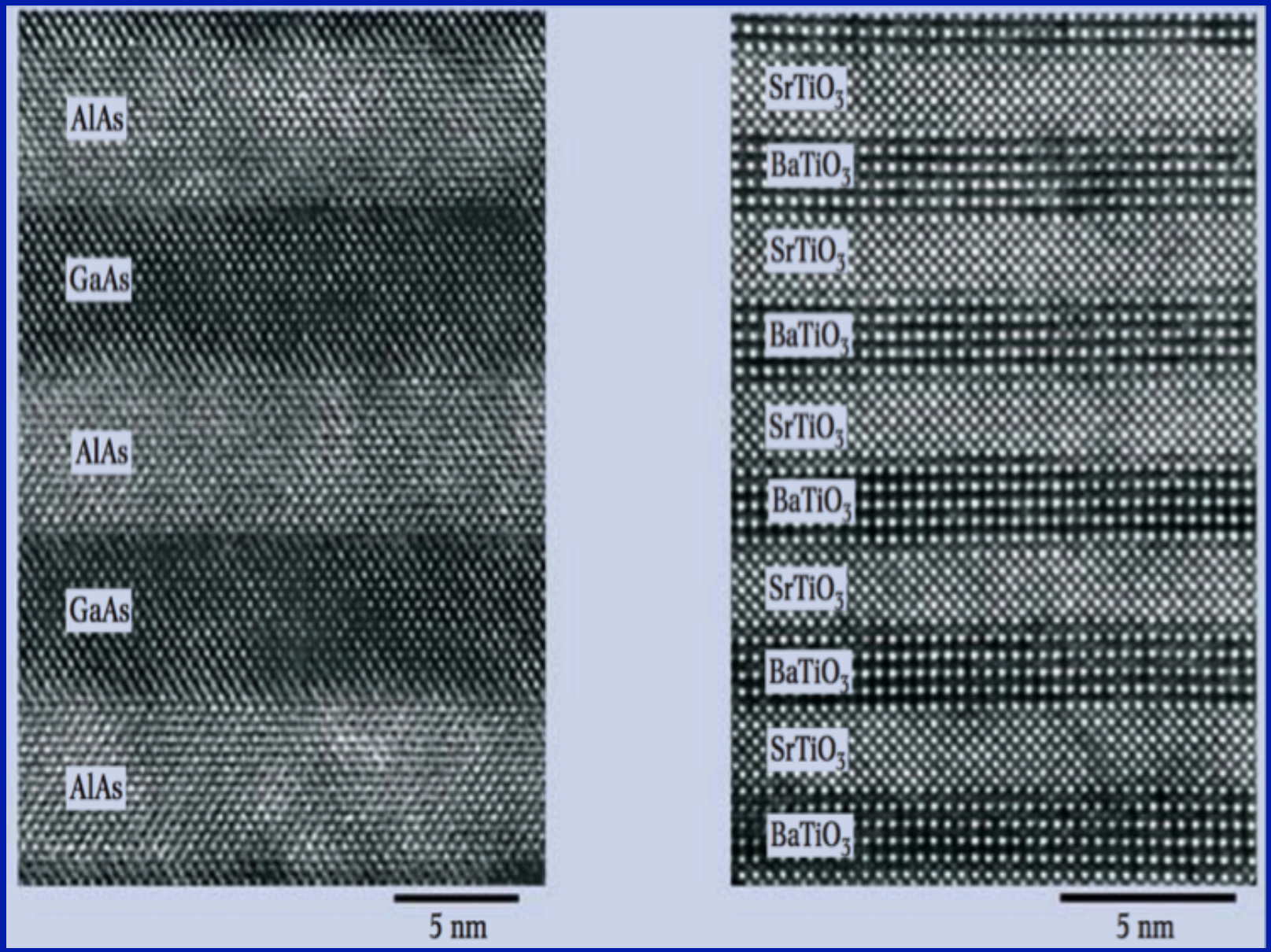

A.K. Gutakovskii *et al.* (1995)

D.G. Schlom *et al.* (2001)

Focus on one example: Control of MIT in Nickelates $RNiO_3$

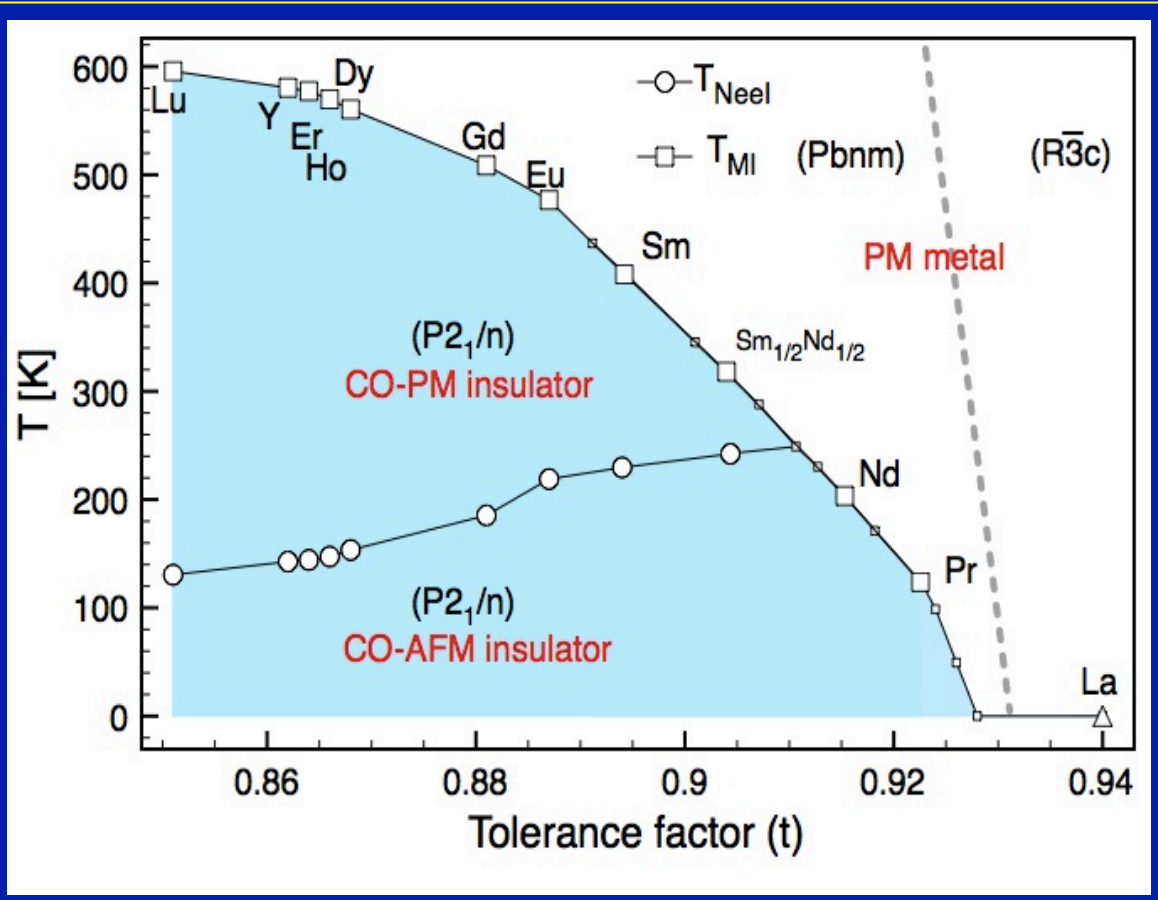

R.Scherwitzl PhD Thesis Geneva 2012 (credit for several slides below)

$$t = \frac{d_{\mathrm{R-O}}}{\sqrt{2}d_{\mathrm{Ni-O}}}$$

57	58	59	60	61	62	63	64	65	66	67	68	69	70	71
La	Ce	Pr	Nd	Pm	Sm	Eu	Gd	Tb	Dy	Ho	Er	Tm	Yb	Lu

R.Sherwitzl, PhD thesis Adapted from Catalan, *Phase Transitions*, (2008)

Control by strain

Resistivity of a thick film
Can this be controlled by
changing substrate (strain) ?

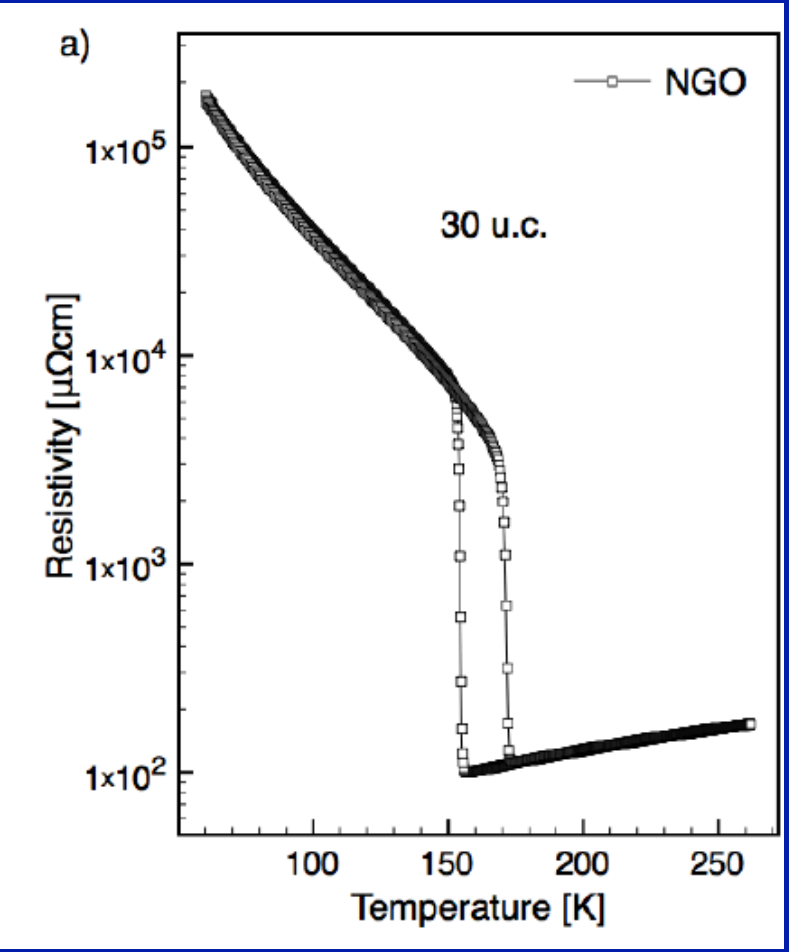

Pressure studies on bulk: encouraging.
Canfield et al. PRB (1993)
P= 1, 5.2, 9.0, 10.8, 14.1 kbar

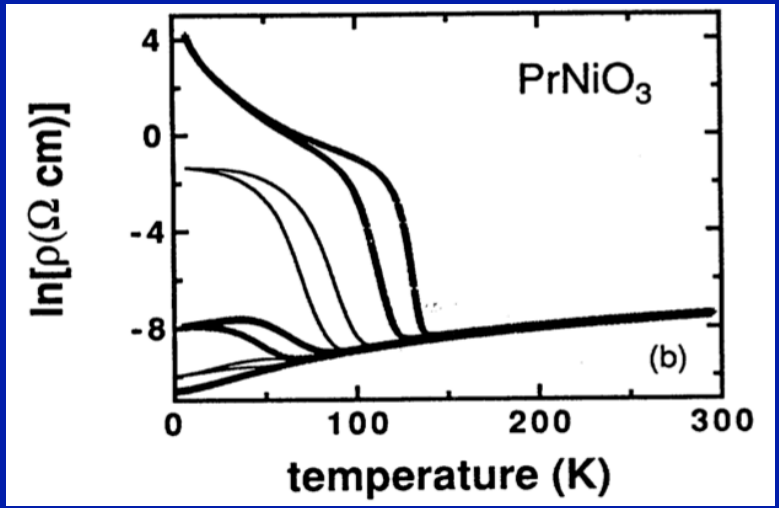

Growth of $RNiO_3$

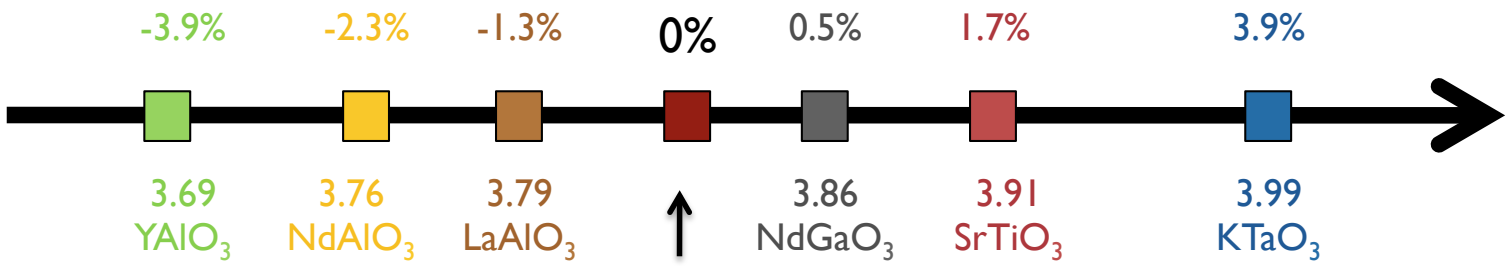

$LaNiO_3$: 3.84 Å pc

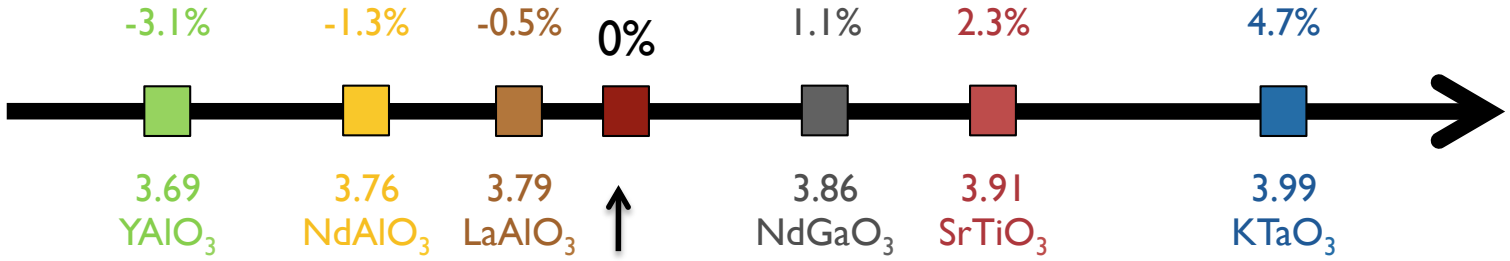

$NdNiO_3$: 3.81 Å pc

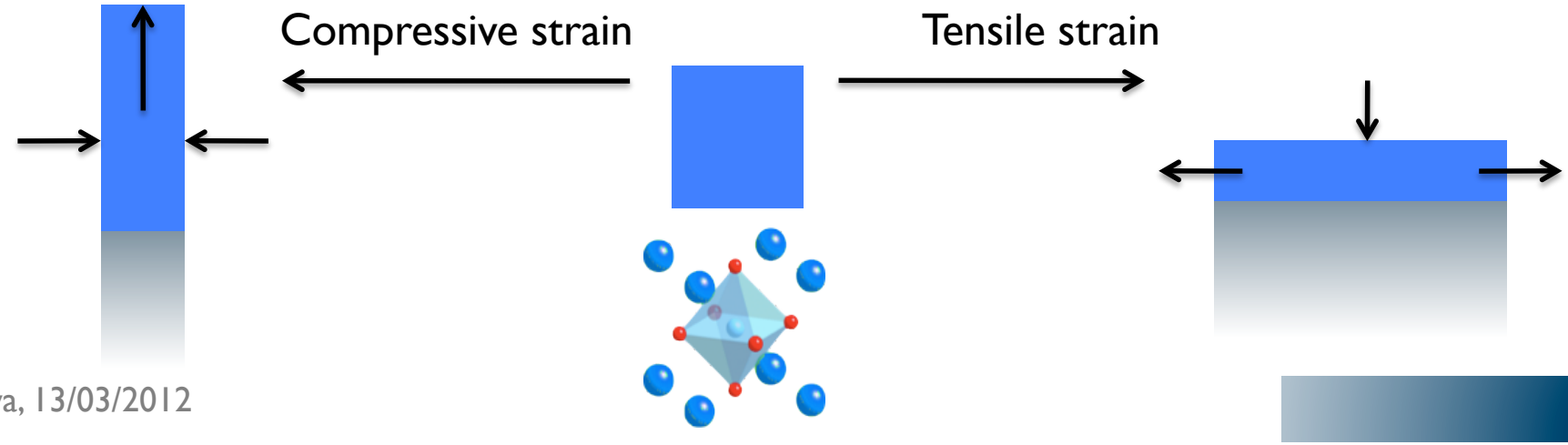

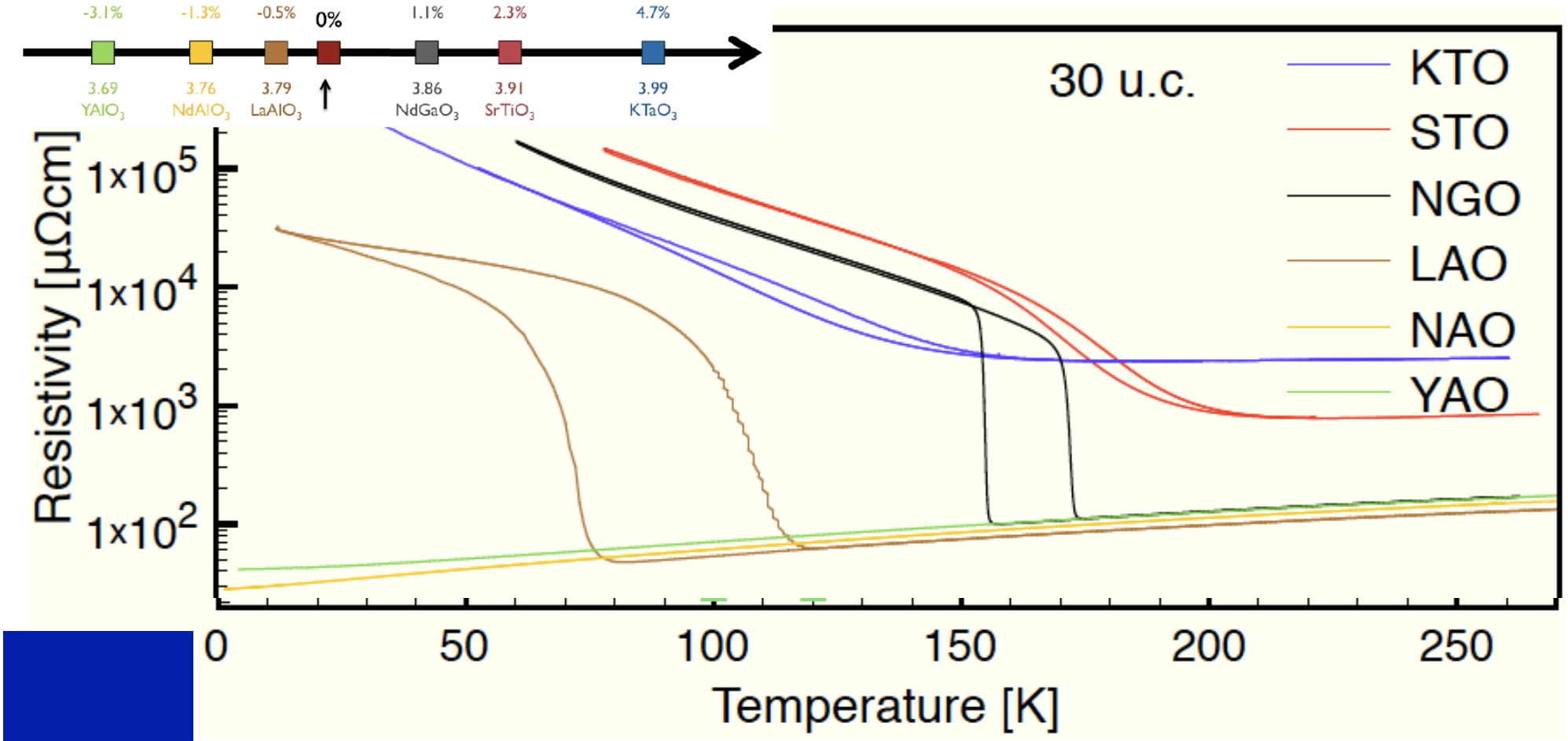

Compressive strain:

- Does not change much resist in metallic state (~ 50%)
- Efficiently shifts MIT to lower T, even complete suppression: → NNO ~ LAO

Tensile strain:

- Increases resist in metallic phae
- Smaller shift of MIT to higher T (except KTO: disorder ?)

We lack complete knowledge of how strain affects the structure…

Theory (ab-initio) is useful here…
Improved diffraction/spectroscopy on thin samples badly needed…

Strain:
- Changes bandwidth
- Affects orbital splitting
- Disorder complicates things…

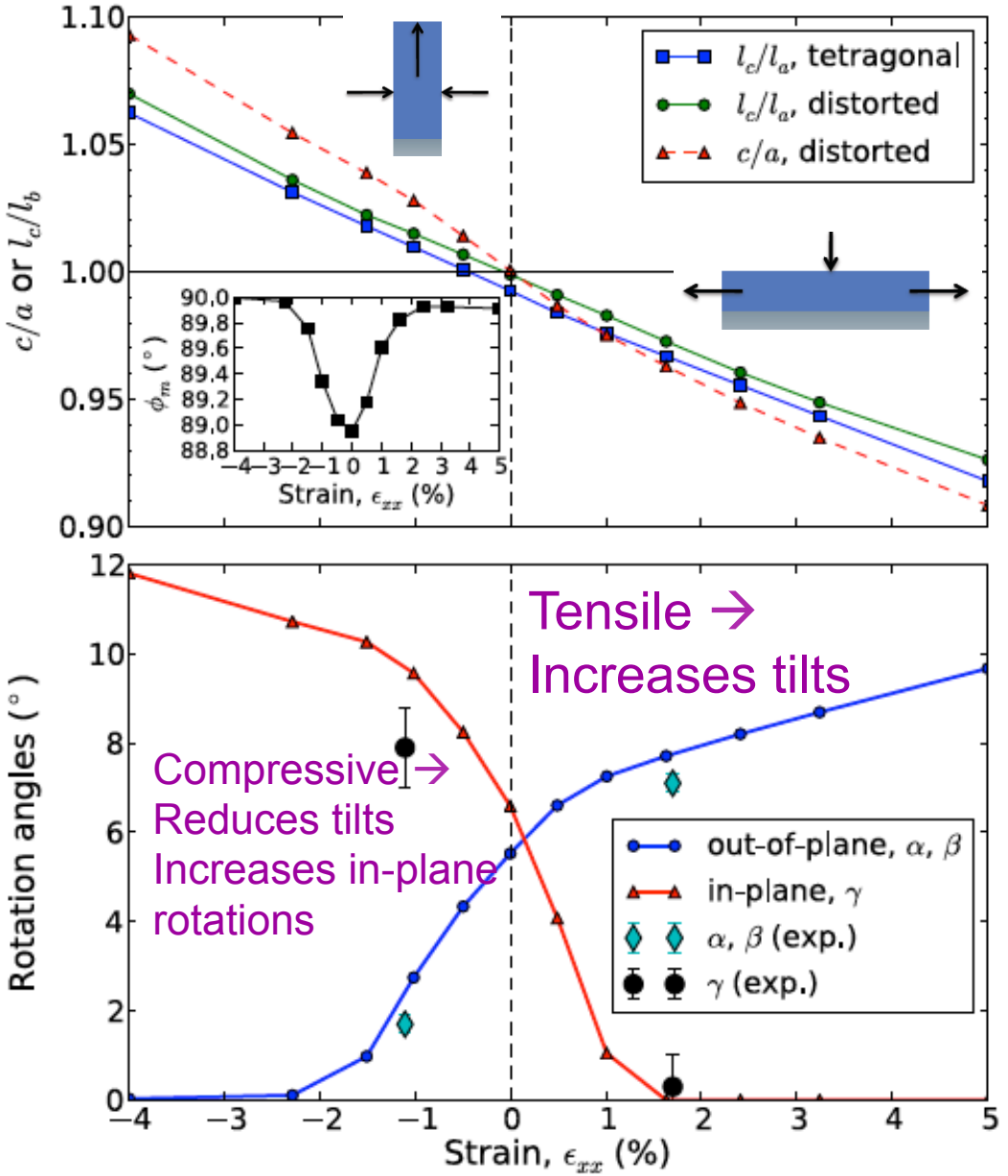

FIG. 1. (Color online) Top: Bond-length ratio, l_c/l_a, for the distorted (solid green) and tetragonal (solid blue) structures under strain. The broken line displays the c/a ratio for the distorted structure (for the tetragonal structure it is identical to the bond-length ratio). In both cases, the strain is defined with respect to $a_{p,\mathrm{eq}}$ of bulk LNO; the shift of the zero-strain point in the tetragonal case reflects thus the difference in the lattice constants of the two types of structures. Bottom: Dependence of the octahedral in-plane rotations (γ) and out-of-plane tilts ($\alpha = \beta$) on strain for the fully relaxed distorted structure. Also, structural refinement data from Ref. [46] are shown with diamonds for $\alpha = \beta$ and with circles for γ. Inset: Inclination angle ϕ_m of the pseudocubic axis c_p with respect to the ab plane.

O.Peil, M.Ferrero & A.G. PRB 2014
cf. also May et al PRB 2010

Control by gating/electric field
from conventional FETs to ionic liquids

- K. Ueno *et al.*, *Nature Materials*, (2008)
- J.T.Ye *et al.*, *Nature Materials*, (2009)
- Y.Yamada *et al.*, *Science*, (2011)
- K. Ueno *et al.*, *Nat. Nano.*, (2011)

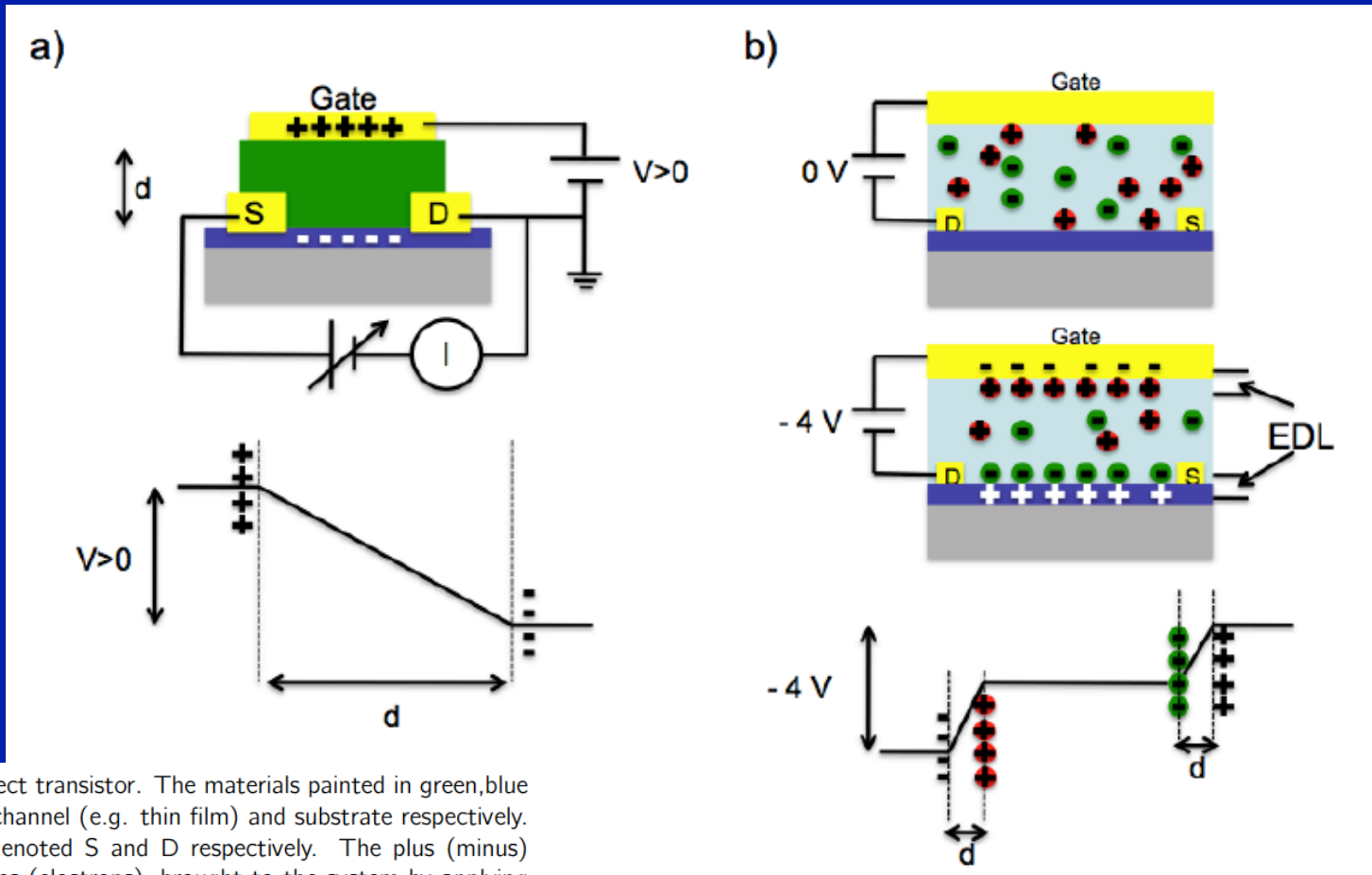

Fig. 4.4: a) Conventional top-gate field-effect transistor. The materials painted in green,blue and grey correspond to the dielectric, the channel (e.g. thin film) and substrate respectively. Source and drain contacts in yellow are denoted S and D respectively. The plus (minus) signs corresponds to electrical charges, holes (electrons), brought to the system by applying a voltage V to the gate. A voltage is applied at the same time between the source and the grounded drain contact and the current is measured. Below, a sketch of the voltage drop across the dielectric across its thickness d. b) Liquid-gate field-effect transistor with 0 V and -4 V applied. The red and green charges represent cations and anions respectively. With applied gate voltage two electric double layers (EDL) form. The voltage drop across the liquid is sketched below.

Carrier modulation of 10^{14}-10^{15} cm^{-2} can be achieved ! (~ 3 orders of mag. larger than with SiO_2 gating)

Some spectacular experiments…

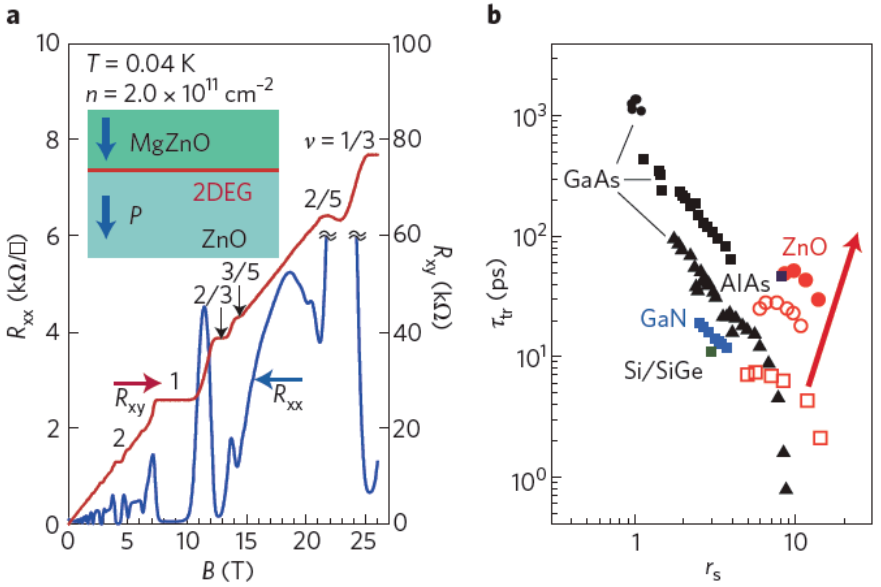

Figure 8 | Fractional quantum Hall effect in ZnO. a, Longitudinal resistance R_{xx} (blue) and Hall resistance R_{xy} (red) of a 2DEG formed at a MgZnO/ZnO interface. Inset: depicts a cross-sectional schematic of the heterostructure. **b**, Comparison of 2DEGs in various semiconductors as functions of the electron–electron interaction strength represented by the Wigner–Seitz radius r_s and transport scattering time τ_{tr}. Data are derived from Fig. 2 of ref. 81 except for the solid red circles, obtained for the sample shown in **a**. The arrow indicates the direction of progress in pursuing a regime of parameters in ZnO that are hard to access in other semiconductors. Panels adapted with permission from: **a**, ref. 83, © 2011 APS; **b**, ref. 81, © 2010 NPG.

FQHE in a ZnO/MgZnO 2DEG
Tsukazaki et al. Nat.Mat. 2010

Field-induced /control of super- -conductivity

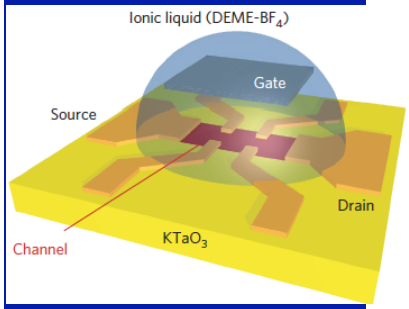

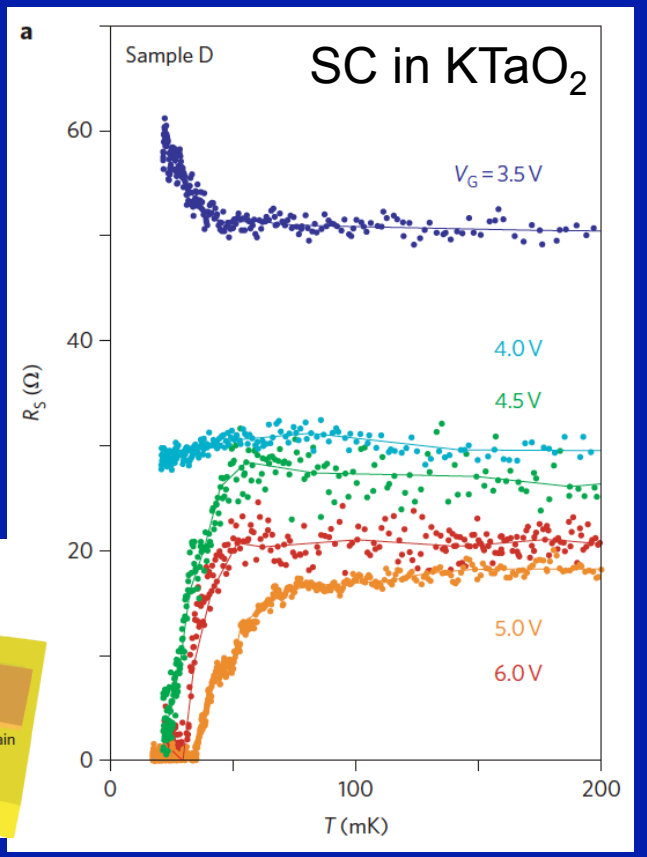

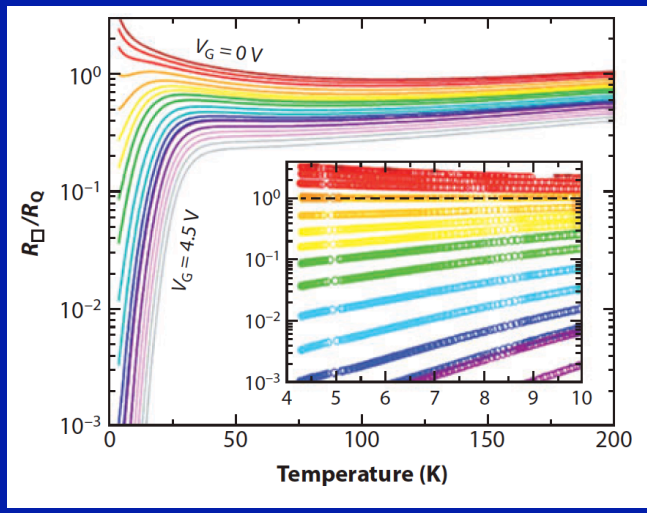

Gating of LSCO cuprate (Bozovic et al.)

Field-control of MIT in $NdNiO_3$ on $LaAlO_3$

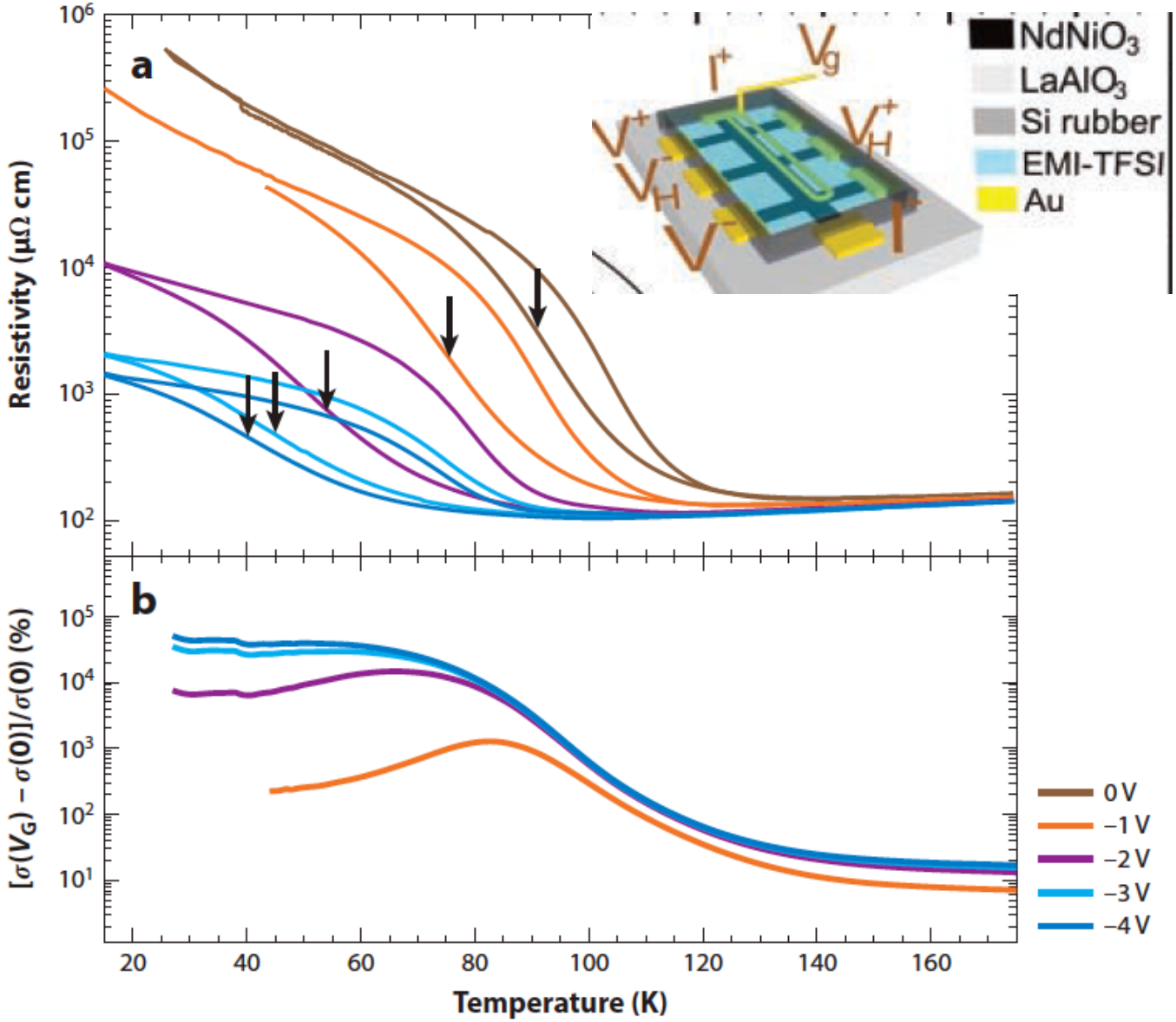

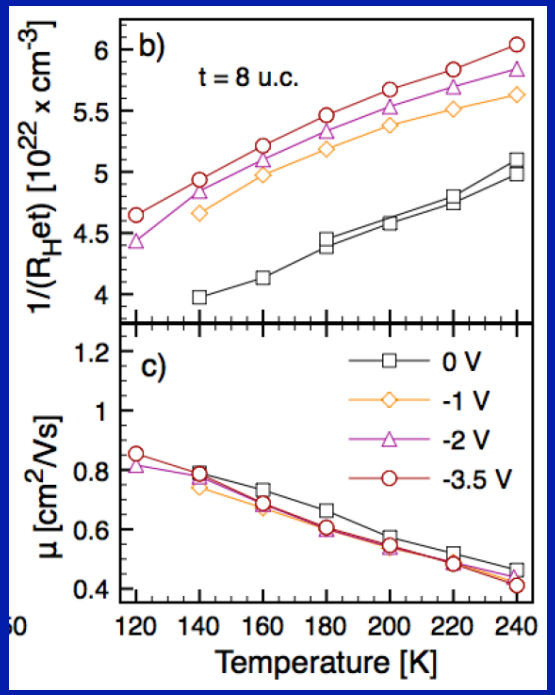

R.Scherwitzl et al.
Adv. Mat. 22, 5517 (2010)

Electric field control of a metal-insulator transition. (*a*) Modulation of the metal-insulator transition temperature in ultrathin films of $NdNiO_3$ by using an ionic liquid gate. Arrows represent the nominal transition temperature of the metal-insulator transition. (*b*) Electroconductivity as a function of temperature and applied gate voltage. Reproduced with permission from Reference 26.

Towards applications…

- Bolometers
- `Piezoelectronic' transistor (PET / IBM)
- ``Synaptic'' devices
- Control of MIT by voltage pulses

→ Resistive RAMs

International Technology Roadmap for Semiconductors - 2013

Emerging Research Materials Summary Table	
Difficult Challenges 2013-2020	*Summary of Issues*
Achieving desired properties in integrated structures	Identify integrated high k dielectrics with EOT <0.5nm and low leakage Identify integrated contact structures that have ultralow contact resistivity Achieving high hole mobility in III-V materials in FET structures Achieving high electron mobility in Ge with low contact resistivity in FET structures Achieving a bandgap in graphene in FET structures Multiferroic with Curie temperature >400K and high remnant magnetization to >400K Ferromagnetic semiconductor with Curie temperature >400K Synthesis of CNTs with tight distribution of bandgap and mobility Electrical control of the electron correlation, ex. Mott transition, Spin dynamics Simultaneously achieve package polymer CTE, modulus, electrical, thermal properties, with moisture and ion diffusion barriers Thermal interface materials with low interface thermal resistance and high thermal conductivity with desired electrical and mechanical properties. Nanosolders compatible with <200C assembly, multiple reflows, high strength, and high electromigration resistance NanoInks that can be printed as die attach adhesives with required electrical, mechanical, thermal, and reliability properties. NanoInks that can be printed as conductors, via hole fillers, solders, or die attach adhesives with required electrical, mechanical, thermal, and reliability properties.
Characterize and control coupled properties of embedded materials and their interfaces	High mobility transition metal dichalcogenides TMD with unpinned Fermi level and low resistance ohmic contacts High electron mobility in Ge with unpinned Fermi level and low resistance ohmic contacts High mobility in nanowires with unpinned Fermi level Graphene with a bandgap, high mobility, and unpinned Fermi level at dielectric interfaces Complex metal oxides with unpinned Fermi levels Nanoscale observation of the magnetic domain structure, for example, the domain in STT-RAM under the magnetic field, i.e., the dynamic operation Characterization of electrical properties of molecule / metal contact interfaces (i.e. Pentacene/Au) Characterization of electrical properties of embedded nano contact interfaces (i.e. CNT/Metal) CNTs with low resistance contacts on both ends

Future transistors

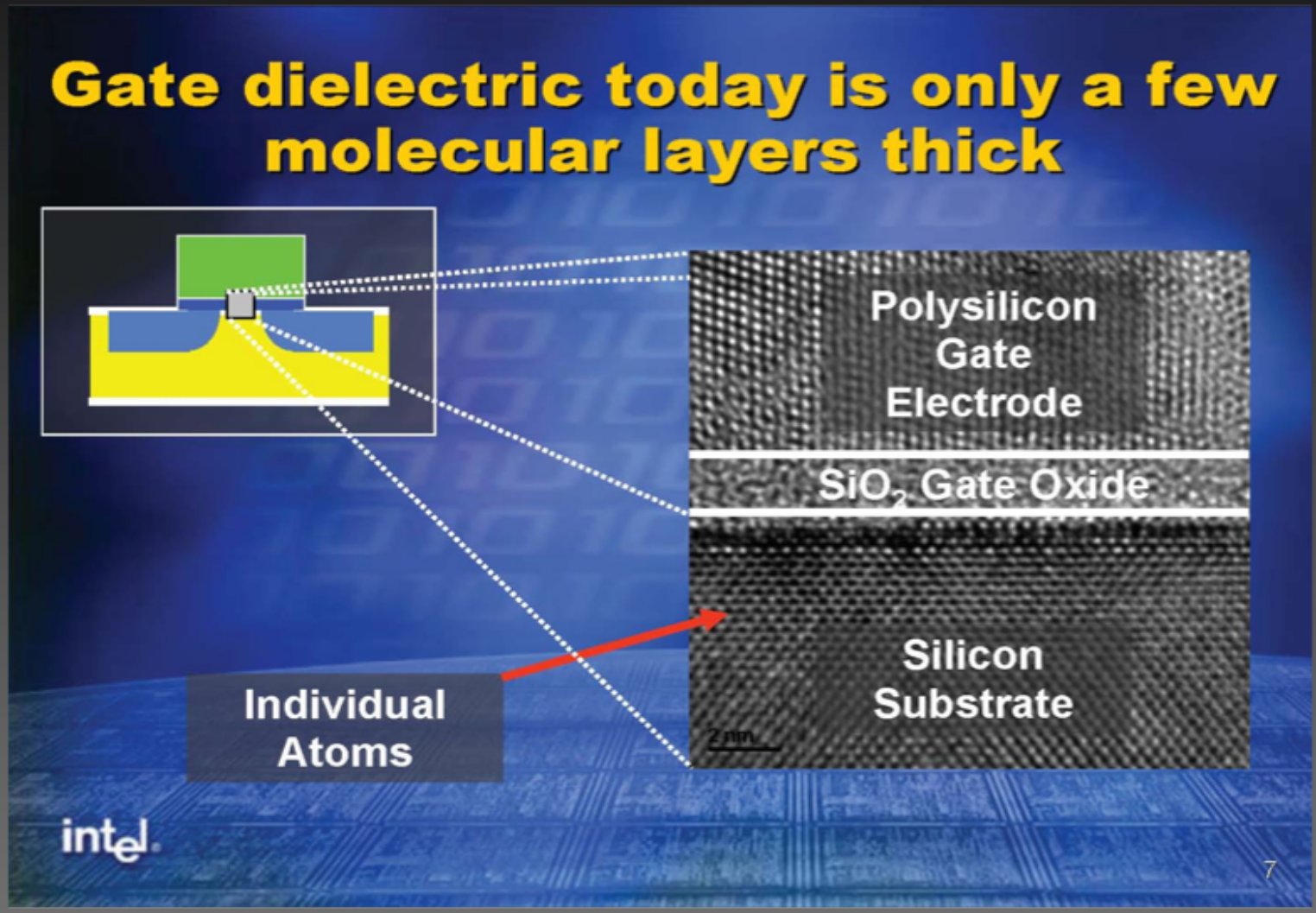

This slide (and 2 next): courtesy J-M. Triscone

Energy densities

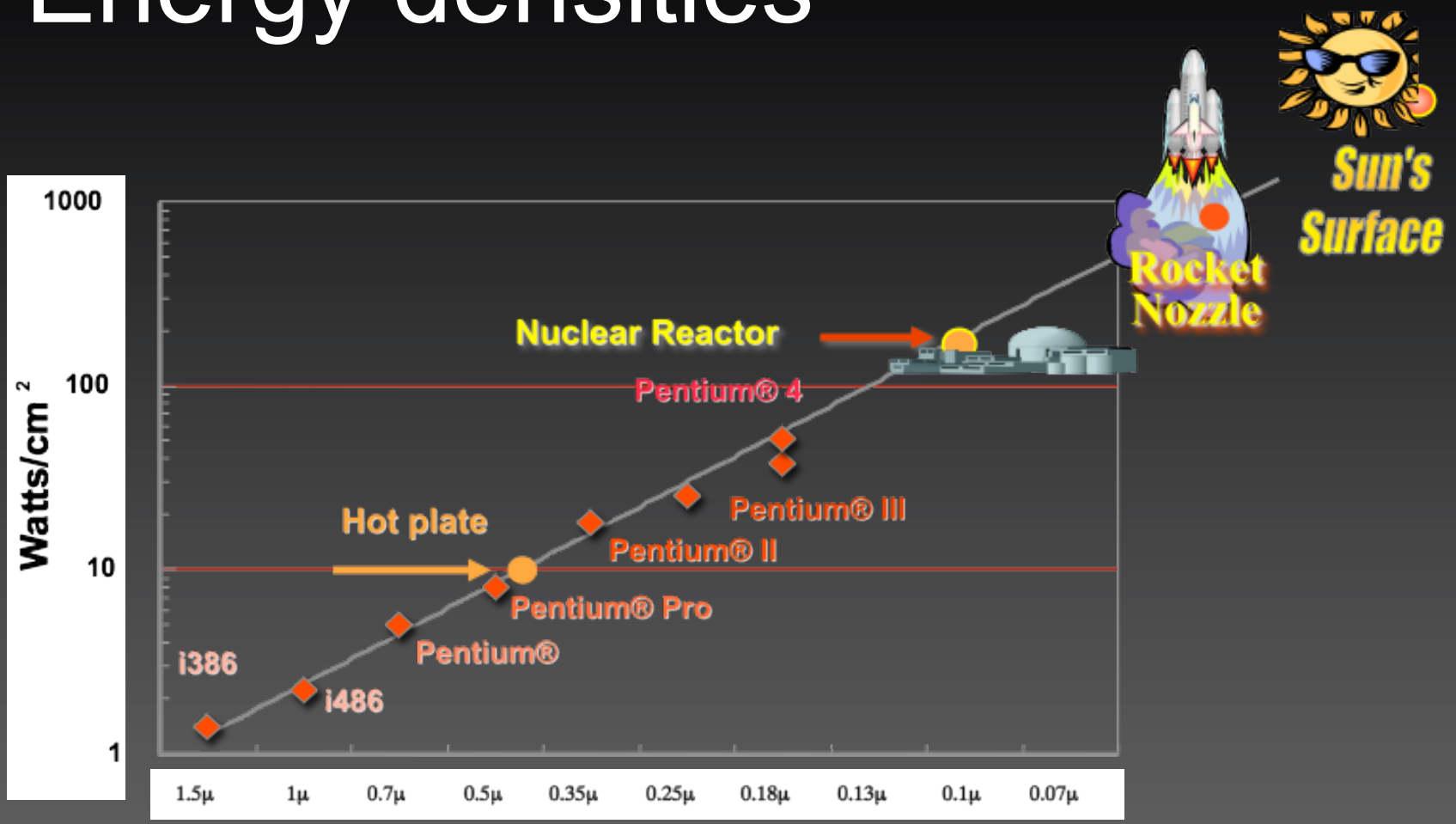

"New Microarchitecture Challenges in the Coming Generations of CMOS Process Technologies" – Fred Pollack, Intel Corp. Micro32 conference key note - 1999. Courtesy Avi Mendelson, Intel.

Viewgraph from http://www-unix.ecs.umass.edu/~mheath/

PET transistor - the future «CMOS» technology?

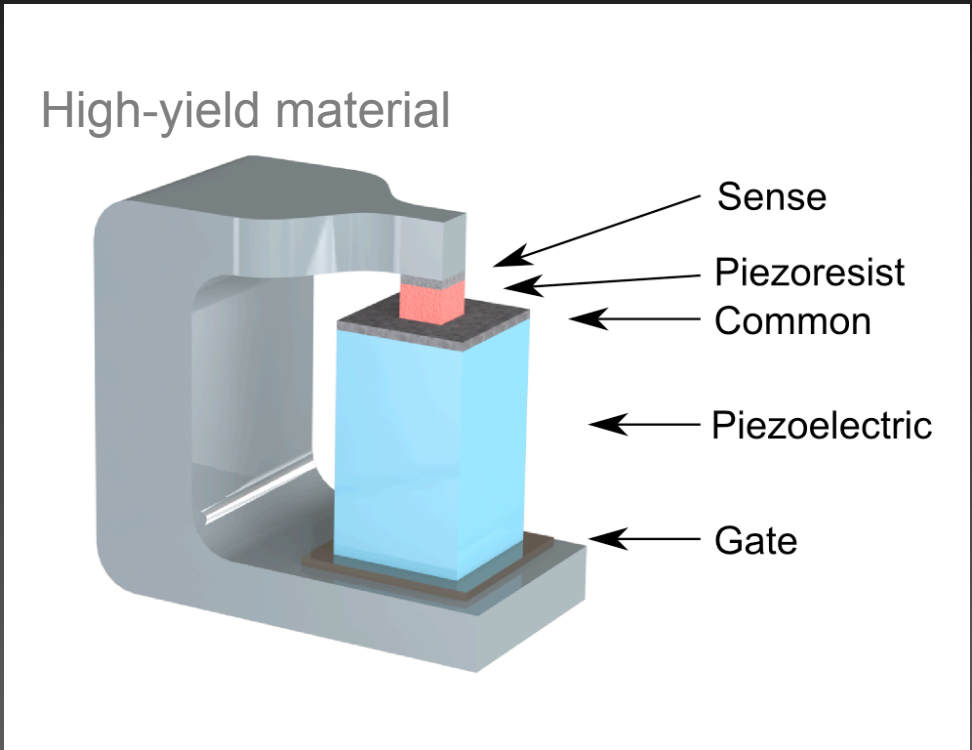

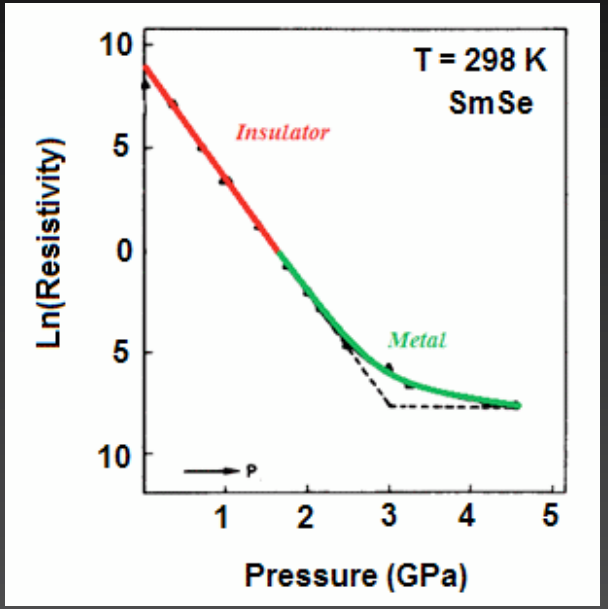

Piezoresistive SmSe:
Unexpected byproduct of f-electron mixed valence basic research !

`Hammer and nail' effect: piezo converts small voltage to strain
→ piezoresitive element switches and activates the device

D.Newns et al. (IBM) in e.g. Adv Mat 2012, JAP 2012 estimate GHz operating cycle at low (0.1 V) operating voltage

``Orbital engineering'' in oxides

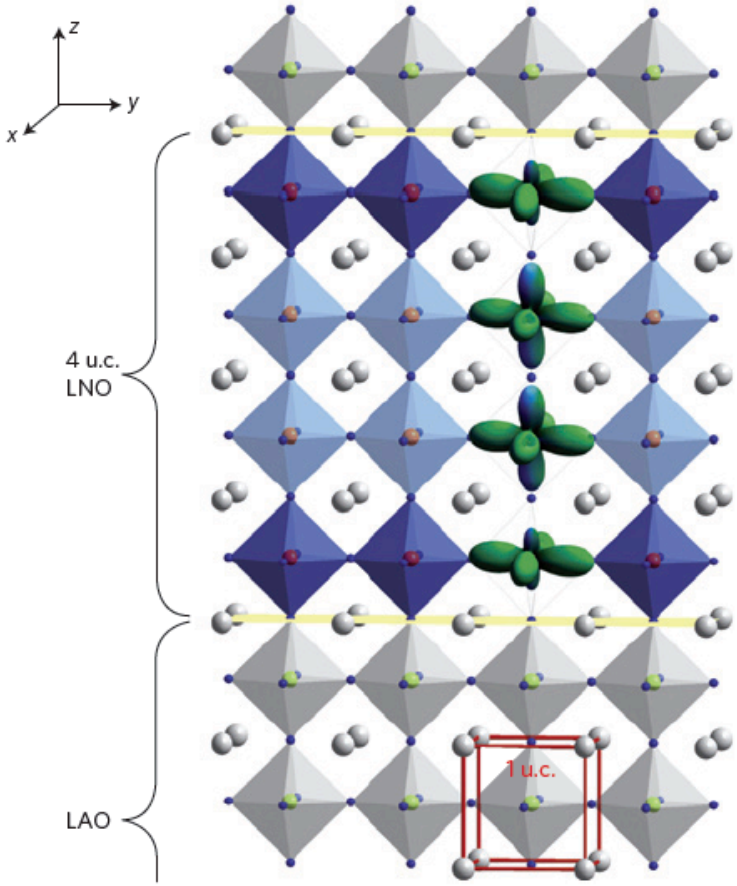

Figure 5 | Heterostructure of metallic $LaNiO_3$ with partially occupied Ni e_g orbitals (LNO, blue) and insulating $LaAlO_3$ (LAO, white)[46]. The orbital polarization at the interface (x^2-y^2 shown in green and $3z^2-r^2$ shown in dark blue) is exaggerated for clarity. Figure reproduced from ref. 46, © 2011 NPG.

A creative proposal: turning a nickelate into a superconducting cuprate-like material by strain-engineering ?

Chaloupka and Khaliullin, PRL 2008
Hansmann et al., PRL 2010

Today's alchemy… ?

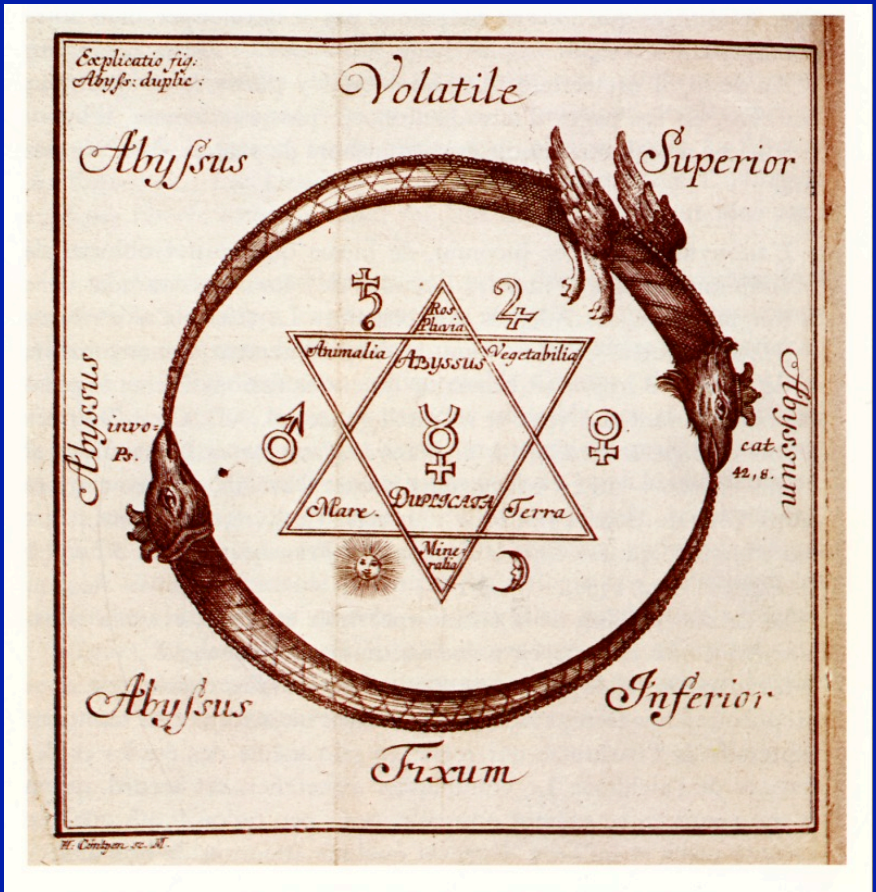

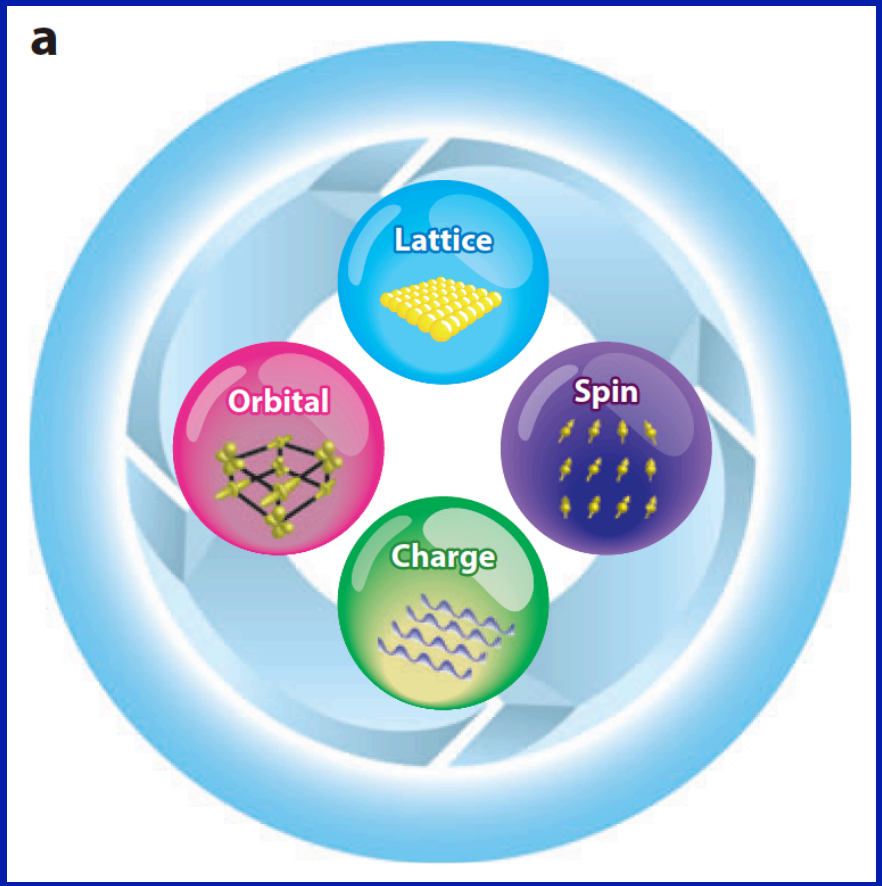

Orbital Order and Possible Superconductivity in $LaNiO_3/LaMO_3$ Superlattices

Jiří Chaloupka[1,2] and Giniyat Khaliullin[1]

[1]*Max-Planck-Institut für Festkörperforschung, Heisenbergstrasse 1, D-70569 Stuttgart, Germany*
[2]*Institute of Condensed Matter Physics, Masaryk University, Kotlářská 2, 61137 Brno, Czech Republic*
(Received 3 July 2007; published 10 January 2008)

A hypothetical layered oxide La_2NiMO_6 where NiO_2 and MO_2 planes alternate along the c axis of ABO_3 perovskite lattice is considered theoretically. Here, M denotes a trivalent cation Al, Ga,... such that MO_2 planes are insulating and suppress the c-axis charge transfer. We predict that correlated e_g electrons in the NiO_2 planes develop a planar x^2-y^2 orbital order driven by the reduced dimensionality and further supported by epitaxial strain from the substrate. Low-energy electronic states can be mapped to a single-band $t - t' - J$ model, suggesting favorable conditions for high-T_c superconductivity.

Turning a Nickelate Fermi Surface into a Cupratelike One through Heterostructuring

P. Hansmann,[1,2] Xiaoping Yang,[1] A. Toschi,[1,2] G. Khaliullin,[1] O. K. Andersen,[1] and K. Held[2]

[1]*Max-Planck-Institut für Festkörperforschung, Heisenbergstrasse 1, D-70569 Stuttgart, Germany*
[2]*Institute for Solid State Physics, Vienna University of Technology, 1040 Vienna, Austria*
(Received 2 July 2008; published 29 June 2009)

Using the local density approximation and its combination with dynamical mean-field theory, we show that electronic correlations induce a single-sheet, cupratelike Fermi surface for hole-doped 1/1 $LaNiO_3/LaAlO_3$ heterostructures, even though both e_g orbitals contribute to it. The Ni $3d_{3z^2-1}$ orbital plays the role of the axial Cu 4s-like orbital in the cuprates. These two results indicate that "orbital engineering" by means of heterostructuring should be possible. As we also find strong antiferromagnetic correlations, the low-energy electronic and spin excitations in nickelate heterostructures resemble those of high-temperature cuprate superconductors.

e_g eigenstates of the cubic system:

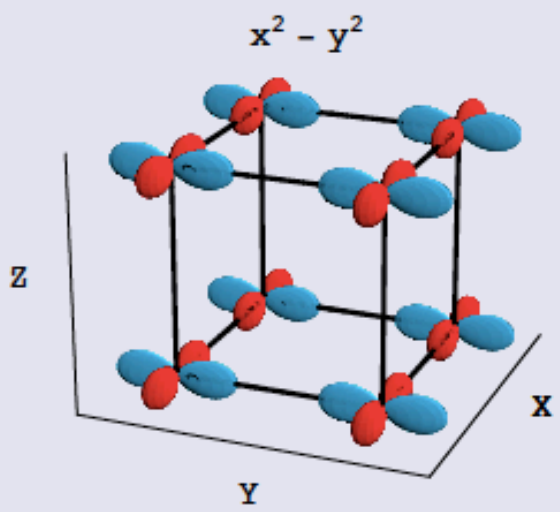

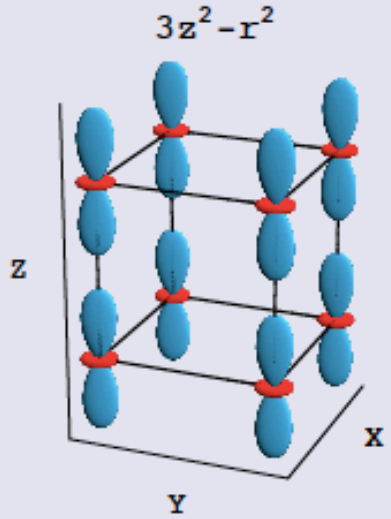

Overlap Integrals (Slater & Koster)

$$t^x = t_0 \begin{pmatrix} \frac{3}{4} & -\frac{\sqrt{3}}{4} \\ -\frac{\sqrt{3}}{4} & \frac{1}{4} \end{pmatrix} \quad t^y = t_0 \begin{pmatrix} \frac{3}{4} & \frac{\sqrt{3}}{4} \\ \frac{\sqrt{3}}{4} & \frac{1}{4} \end{pmatrix} \quad t^z = t_0 \begin{pmatrix} 0 & 0 \\ 0 & 1 \end{pmatrix}$$

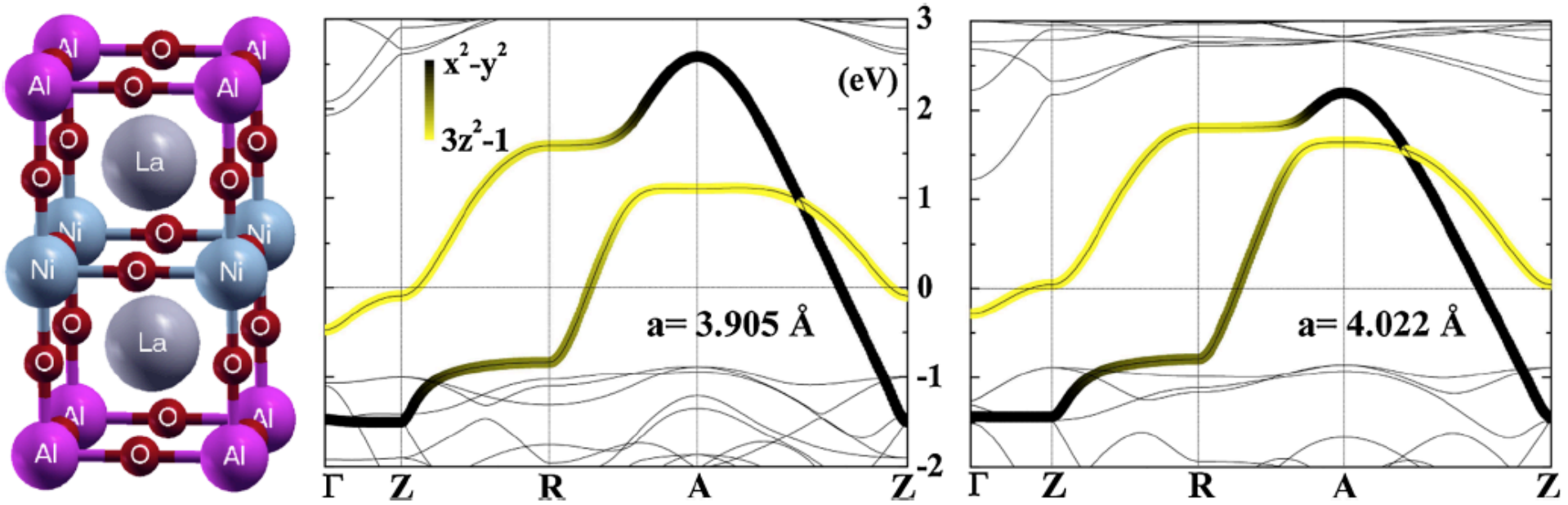

FIG. 1 (color online). The 1/1 $LaNiO_3/LaAlO_3$ heterostructure (left) and its LDA (*N*MTO) band structures without (center) and with (right) strain. The Bloch vector is along the lines $\Gamma(0,0,0) - Z(0,0,\frac{\pi}{c}) - R(0,\frac{\pi}{a},\frac{\pi}{c}) - A(\frac{\pi}{a},\frac{\pi}{a},\frac{\pi}{c}) - Z(0,0,\frac{\pi}{c})$. The shading gives the $x^2 - y^2$ vs $3z^2 - 1e_g$ Wannier-function character.

Band-structure (LDA):
Stabilisation of the x^2-y^2 orbital under tensile strain
Destabilisation of the $3z^2$-r^2 orbital

Naively, interactions enhance orbital polarization

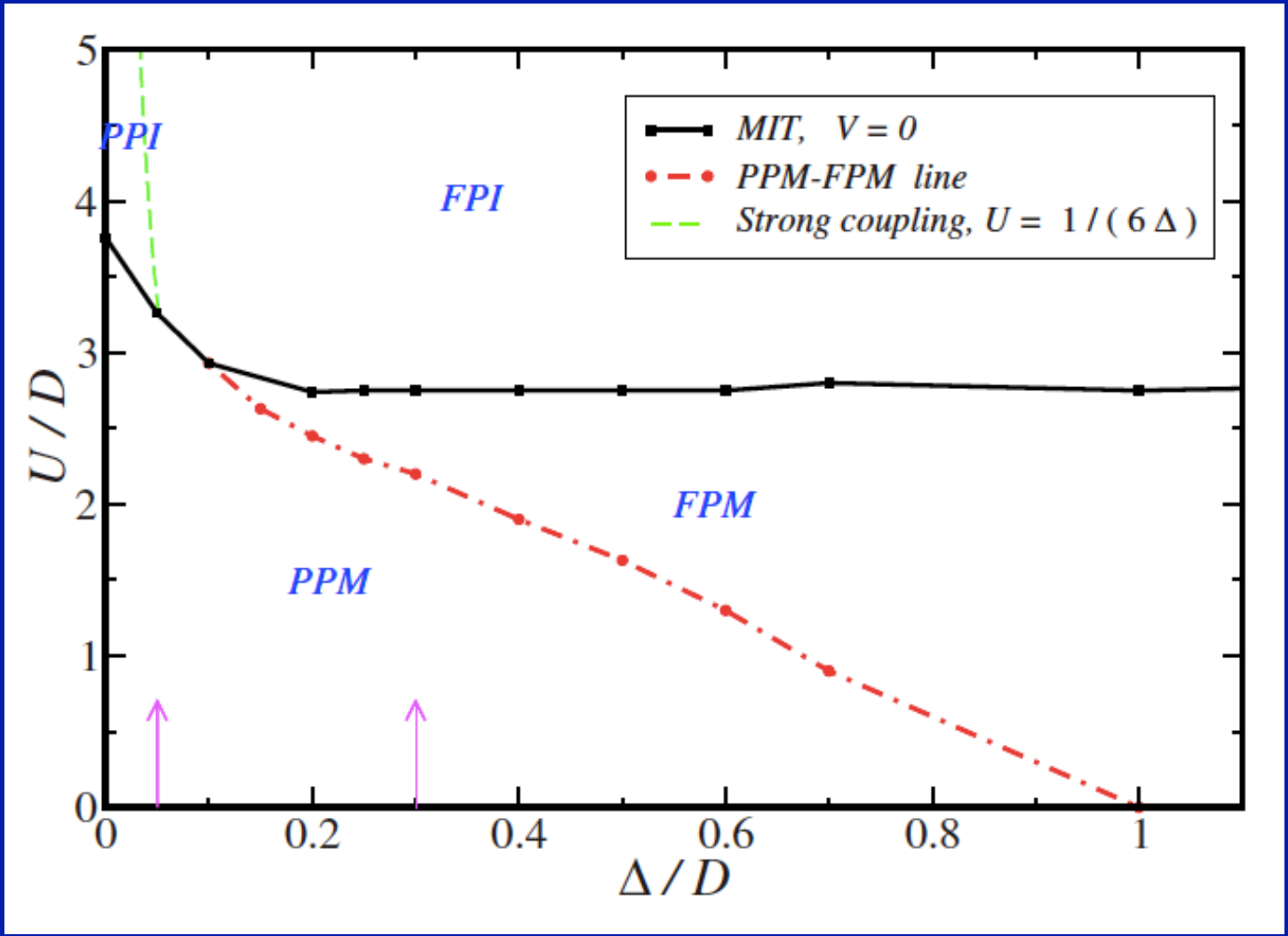

Poteryaev et al. PRB 2008

Hansmann et al. PRL 2009
predict a large orbital polarization → 1-band

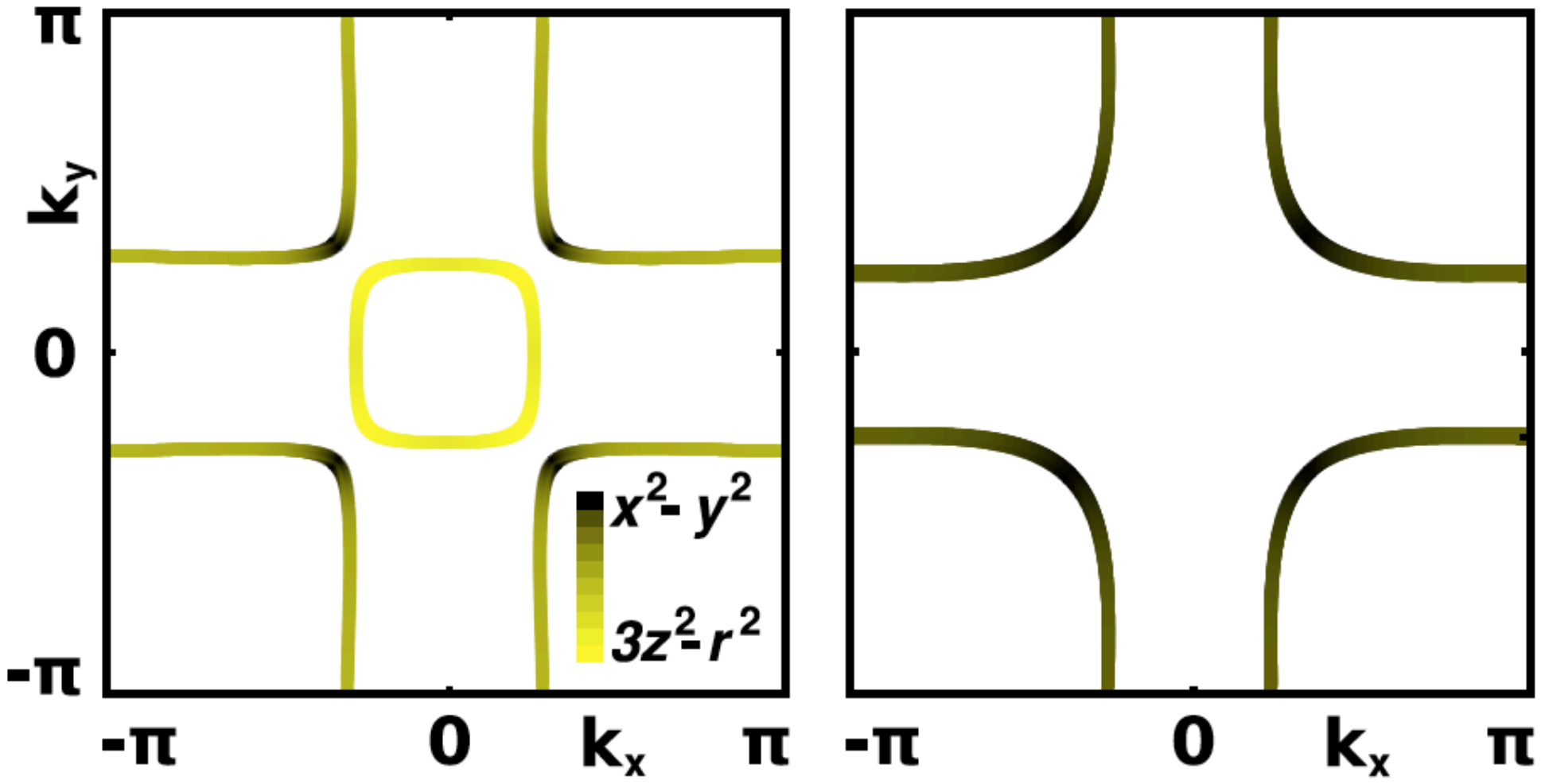

Experiments: Sizeable but far from complete polarization under tensile strain…

PHYSICAL REVIEW B 88, 125124 (2013)

Strain and composition dependence of orbital polarization in nickel oxide superlattices

M. Wu,[1] E. Benckiser,[1,*] M. W. Haverkort,[1,2] A. Frano,[1,3] Y. Lu,[1] U. Nwankwo,[1] S. Brück,[4,5] P. Audehm,[4] E. Goering,[4] S. Macke,[2] V. Hinkov,[2] P. Wochner,[4] G. Christiani,[1] S. Heinze,[1] G. Logvenov,[1] H.-U. Habermeier,[1] and B. Keimer[1,†]

A combined analysis of x-ray absorption and resonant reflectivity data was used to obtain the orbital polarization profiles of superlattices composed of four-unit-cell-thick layers of metallic $LaNiO_3$ and layers of insulating RXO_3 (R = La, Gd, Dy and X = Al, Ga, Sc), grown on substrates that impose either compressive or tensile strain. This superlattice geometry allowed us to partly separate the influence of epitaxial strain from interfacial effects controlled by the chemical composition of the insulating blocking layers. Our quantitative analysis reveals orbital polarizations up to 25%. We further show that strain is the most effective control parameter, whereas the influence of the chemical composition of the blocking layers is comparatively small.

In order to quantitatively analyze the observed dichroism, we applied the sum rule for linear dichroism,[9,21] which relates the ratio of holes in the Ni e_g orbitals to the energy-integrated XAS intensities across the Ni L edge $I_{x,z} = \int_{L_{3,2}} I_{x,z}(E)dE$ for in-plane (x) and out-of-plane (z) polarization, respectively:

$$X = \frac{h_{3z^2-r^2}}{h_{x^2-y^2}} = \frac{3I_z}{4I_x - I_z}. \quad (1)$$

Here, $h_{x^2-y^2}$ and $h_{3z^2-r^2}$ are the hole occupation numbers of orbitals with $x^2 - y^2$ and $3z^2 - r^2$ symmetries.

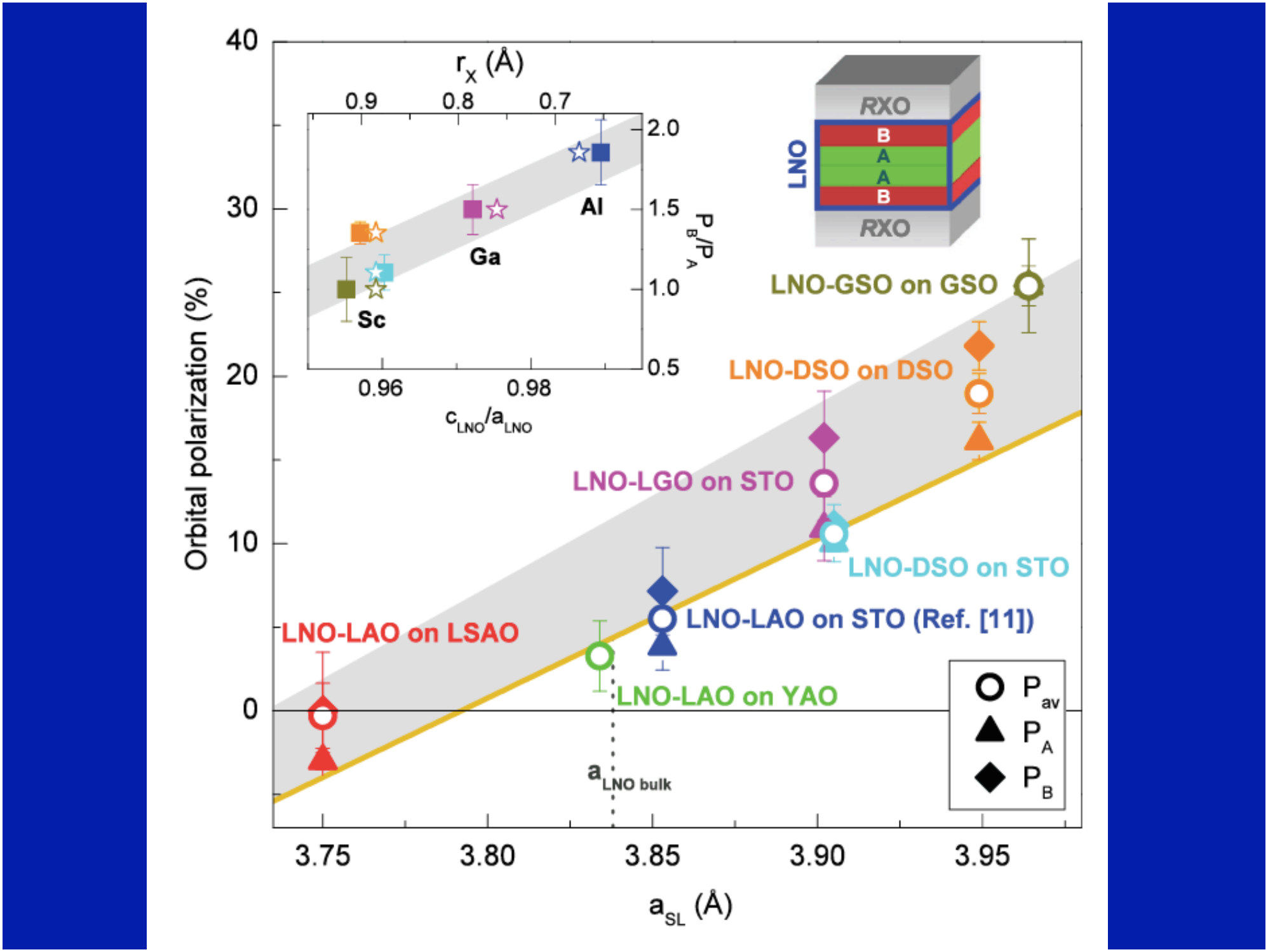
Orbital polarization (%)
40
30
20
10
0
3.75
3.80
3.85
3.90
3.95
a_{SL} (Å)
$a_{LNO\ bulk}$
LNO-LAO on LSAO
LNO-LAO on YAO
LNO-LAO on STO (Ref. [11])
LNO-LGO on STO
LNO-DSO on STO
LNO-DSO on DSO
LNO-GSO on GSO
P_{av}
P_A
P_B
r_X (Å)
0.9
0.8
0.7
Sc
Ga
Al
0.96
0.98
c_{LNO}/a_{LNO}
2.0
1.5
1.0
0.5
P_B/P_A
RXO
B
A
A
B
RXO
LNO

A full LDA+DMFT calculation (taking into account the full set of Ni-d and O-p states) is in good agreement with experiments

See:
LDA+DMFT:
Han et al.
PRL 107, 206804 (2011)
Peil, Ferrero & AG
PRB 2014
Experiments
@MPI-Stuttgart
Wu et al.
PRB 88, 125124 (2013)

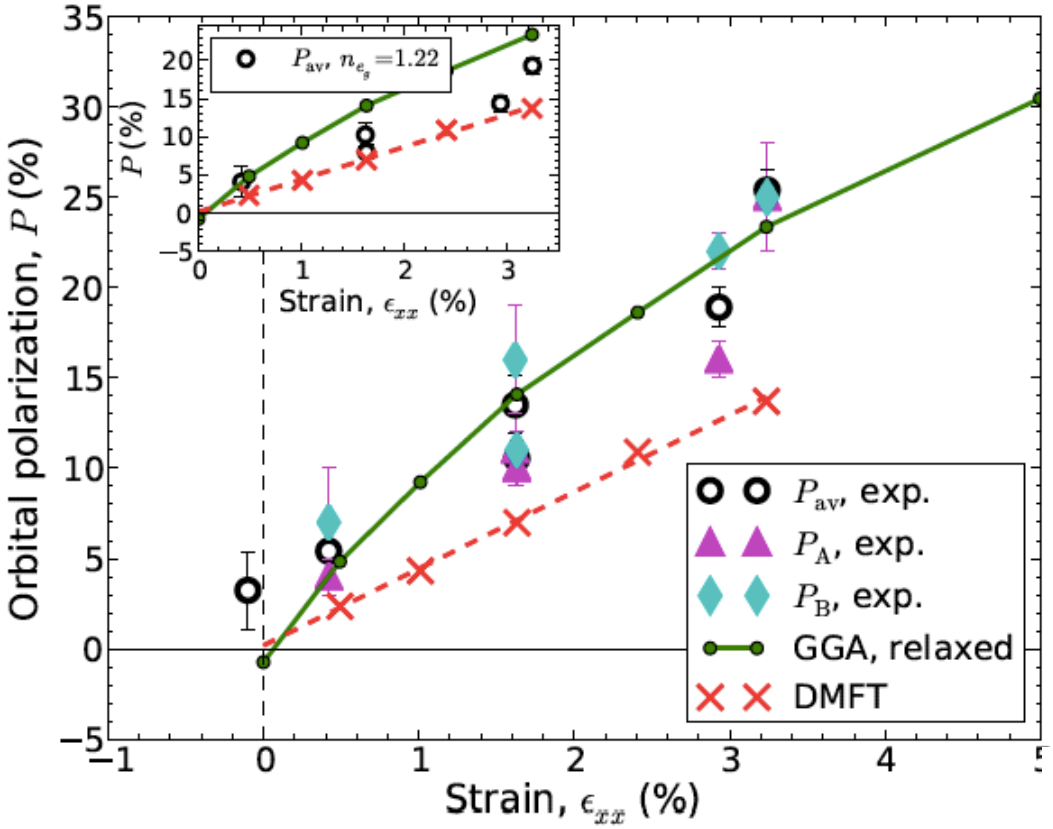

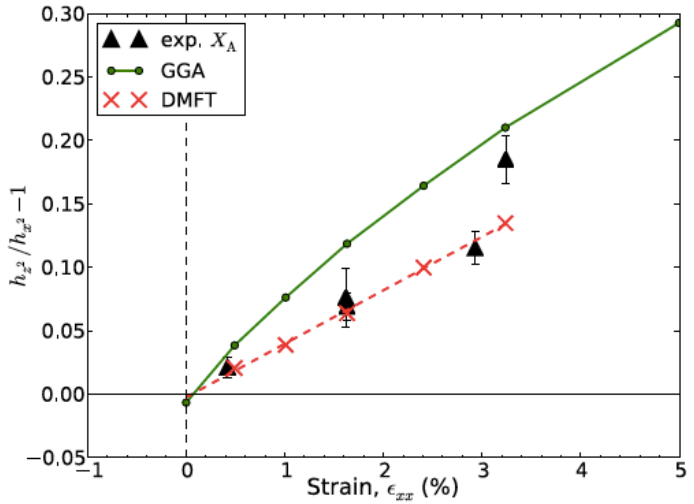

FIG. 12. (Color online) The ratio of the hole occupancies, X, as a function of strain (for experimental points the value for the inner layers, X_A, is used).

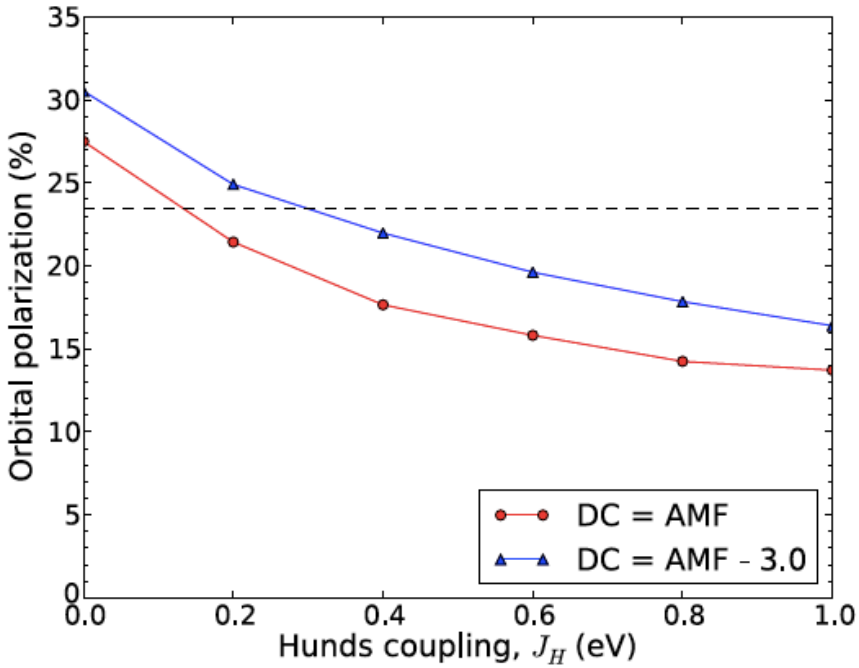

Hund's coupling
fights orbital polarization

What's wrong with the previous prediction and what is this teaching us about the physics of nickelates ?

Contribution of ligand states is crucial
Ni is NOT only (perhaps not primarily)
in Ni^{3+} d^7 state (which would be
Jahn-Teller active → not observed)
Holes form on oxygen and d^8, d^8L^2
configuration become crucial
cf. Mizokawa, Sawatzky, Khomskii

Nature of the insulating phase of nickelates $RNiO_3$

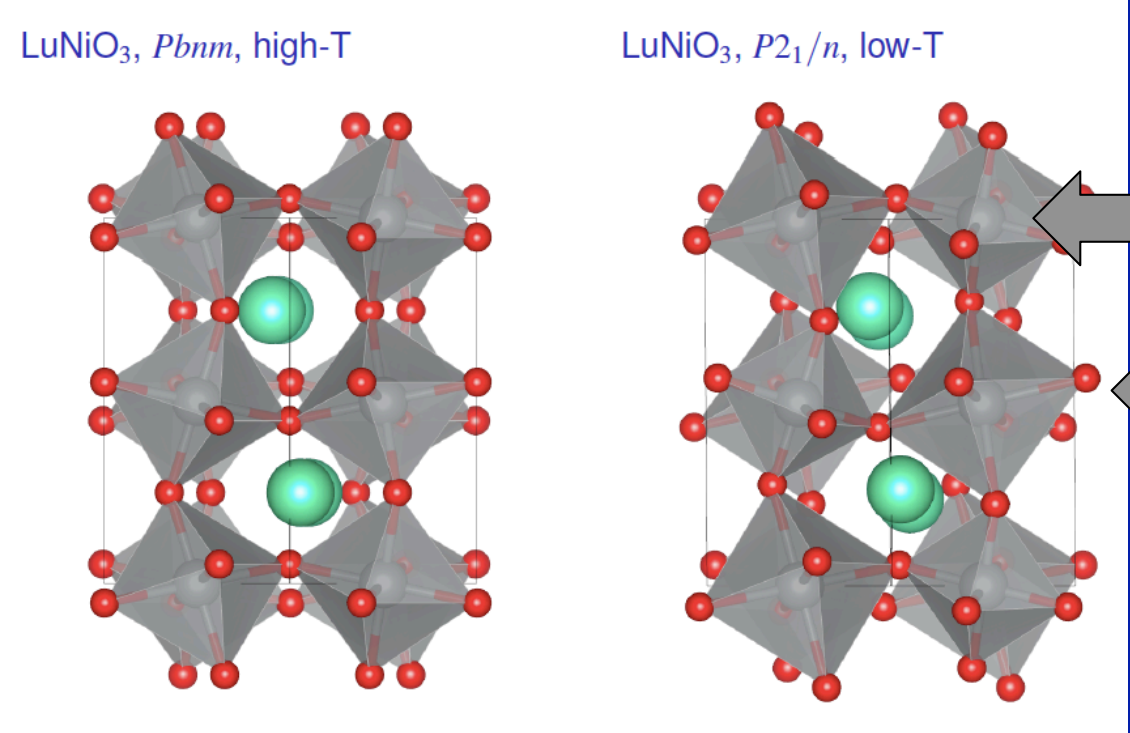

Short-bond octahedron

Long-bond octahedron

Low-T insulating phase:
two types of Ni-site

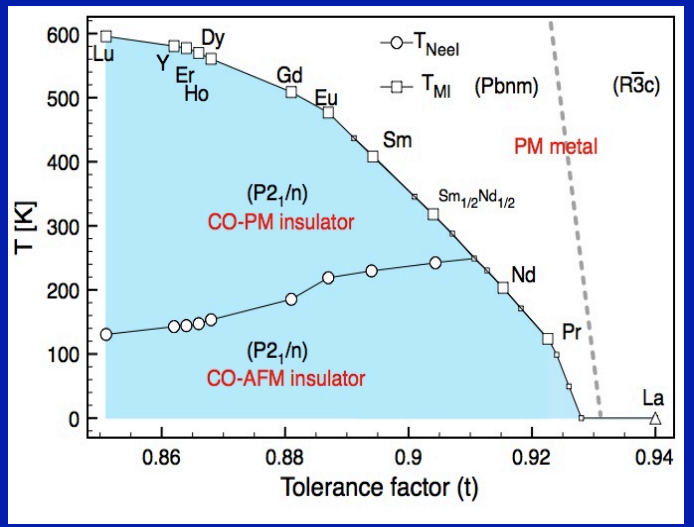

Nominal ionic valence d^7 of Ni^{3+} does NOT apply → Formation of Ligand Holes

Extreme picture:

$$d^7 + d^7 \rightarrow d^8(\mathrm{LB}) + d^8\overline{L}^2(\mathrm{SB})$$

$$e_g^1 + e_g^1 \rightarrow e_g^2 + e_g^0$$

``Bond disproportionation'' (~ charge ordering)
as an alternative way (different from Jahn-Teller)
to lift orbital degeneracy

JOURNAL OF SOLID STATE CHEMISTRY 106, 330–338 (1993)

Additional Oxygen Ordering in "$La_2NiO_{4.25}$" ($La_8Ni_4O_{17}$). II. Structural Features

A. DEMOURGUES, F. WEILL, B. DARRIET, A. WATTIAUX, J. C. GRENIER, P. GRAVEREAU, AND M. POUCHARD

Laboratoire de Chimie du Solide du CNRS, Université de Bordeaux I, 351, Cours de la Libération, 33405 Talence Cedex, France

Received January 11, 1993; in revised form March 25, 1993; accepted March 29, 1993

PHYSICAL REVIEW B VOLUME 61, NUMBER 17 1 MAY 2000-I

Spin and charge ordering in self-doped Mott insulators

T. Mizokawa, D. I. Khomskii, and G. A. Sawatzky

Solid State Physics Laboratory, Materials Science Centre, University of Groningen, Nijenborgh 4, 9747 AG Groningen, The Netherlands

(Received 20 January 2000)

This, unfortunately, limits our ability to favor the x^2-y^2 orbital (at the expense of the $3z^2$-r^2 one) under strain
→ "turning a nickelate into a cuprate"

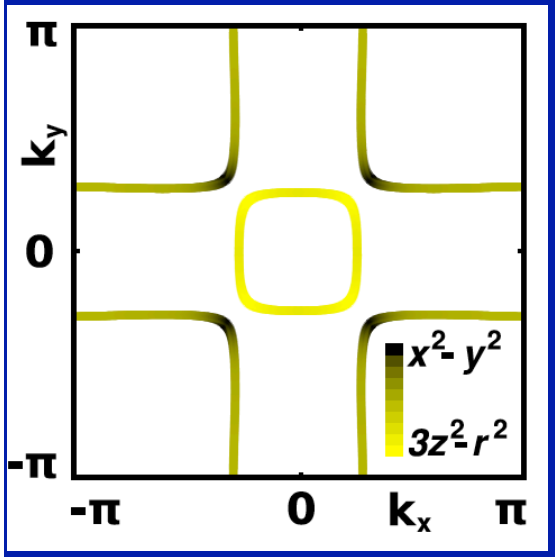

Nickelate--like FS

Tensile strain

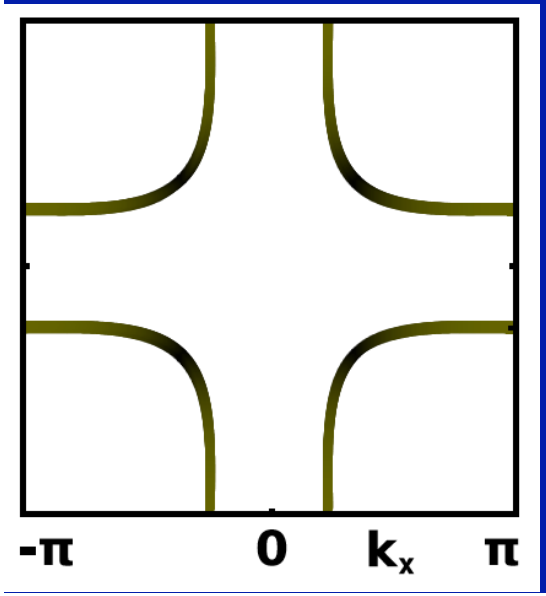

Cuprate --like FS ?

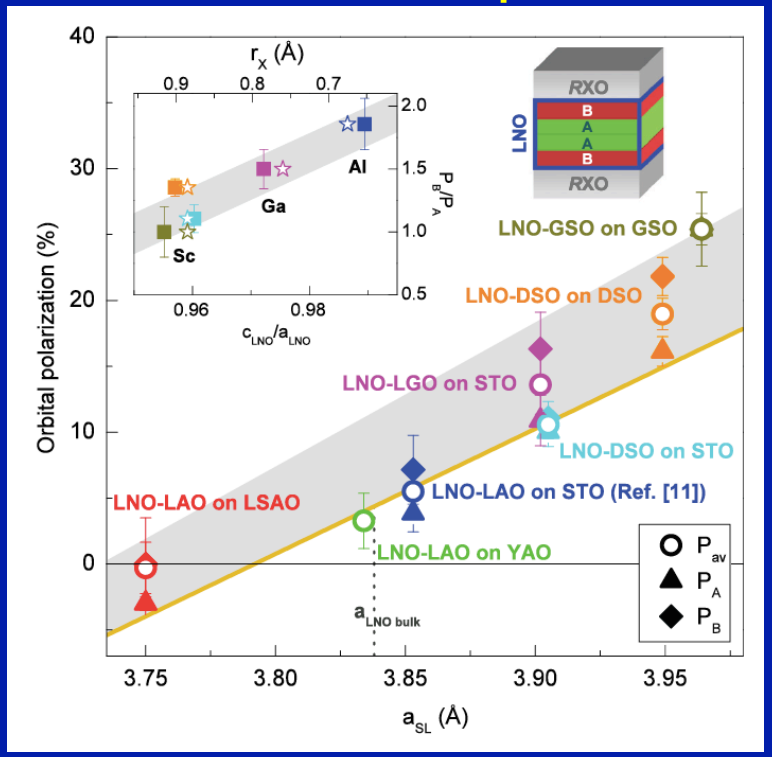

Experiment: Wu et al PRB 2013

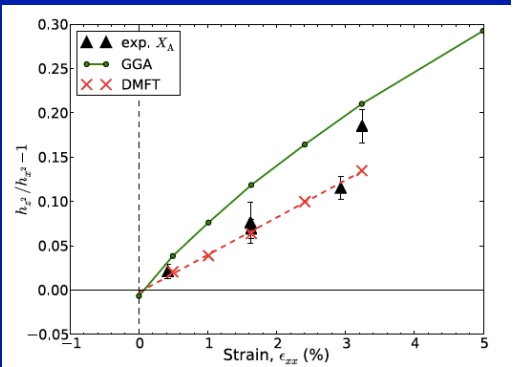

FIG. 12. (Color online) The ratio of the hole occupancies, X, as a function of strain (for experimental points the value for the inner layers, X_A, is used).

Theory: Peil et al. PRB 2014

The physics of the MIT in nickelates CANNOT be understood as a Mott transition of a ¼-filled band !

→ What is the correct 2-band effective low-energy model ?

PHYSICAL REVIEW B 91, 075128 (2015)

Low-energy description of the metal-insulator transition in the rare-earth nickelates

Alaska Subedi,[1,2] Oleg E. Peil,[2,3] and Antoine Georges[2,3,4]

Simplest 2-orbital Model

$$H = -t \sum_{m=1}^{2} \sum_{\sigma=\uparrow,\downarrow} \sum_{\langle ij \rangle} (d^{\dagger}_{m\sigma i} d_{m\sigma j} + h.c.) + H_{\rm int}$$

$$- \frac{\Delta}{2} \sum_{m\sigma, i\in A} d^{\dagger}_{m\sigma i} d_{m\sigma i} + \frac{\Delta}{2} \sum_{m\sigma, j\in B} d^{\dagger}_{m\sigma j} d_{m\sigma j},$$

$$H_{\rm int} = U \sum_{m} \hat{n}_{m\uparrow} \hat{n}_{m\downarrow} + (U-2J) \sum_{m\neq m'} \hat{n}_{m\uparrow} \hat{n}_{m'\downarrow} +$$

$$+(U-3J) \sum_{m<m',\sigma} \hat{n}_{m\sigma} \hat{n}_{m'\sigma} +$$

Key point: Consider this model in the small or negative U-3J regime !

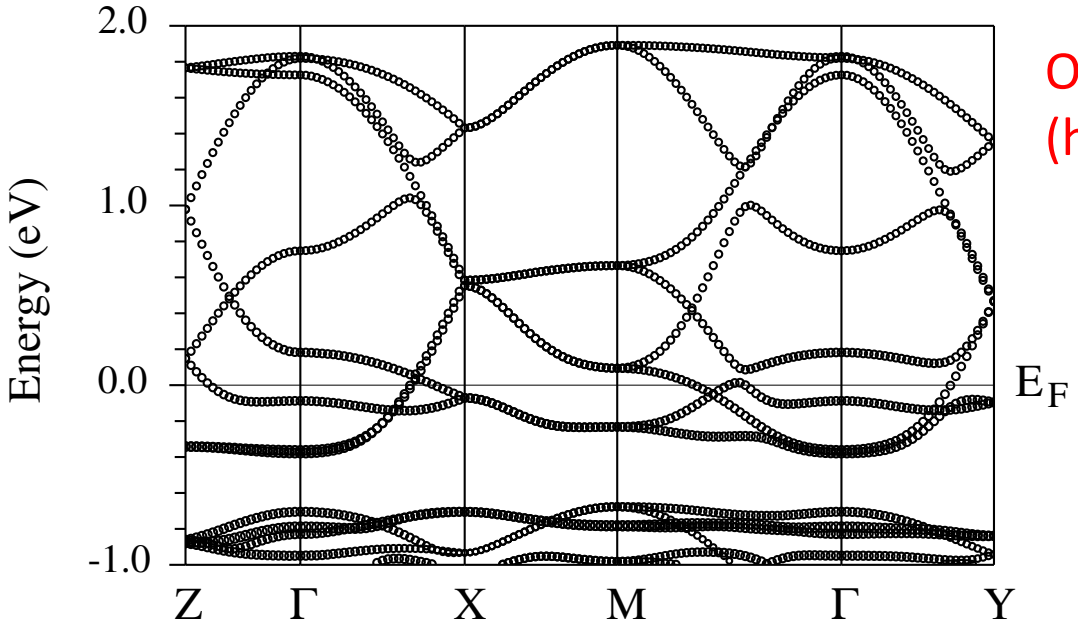

Orthorombic
(hi-T)

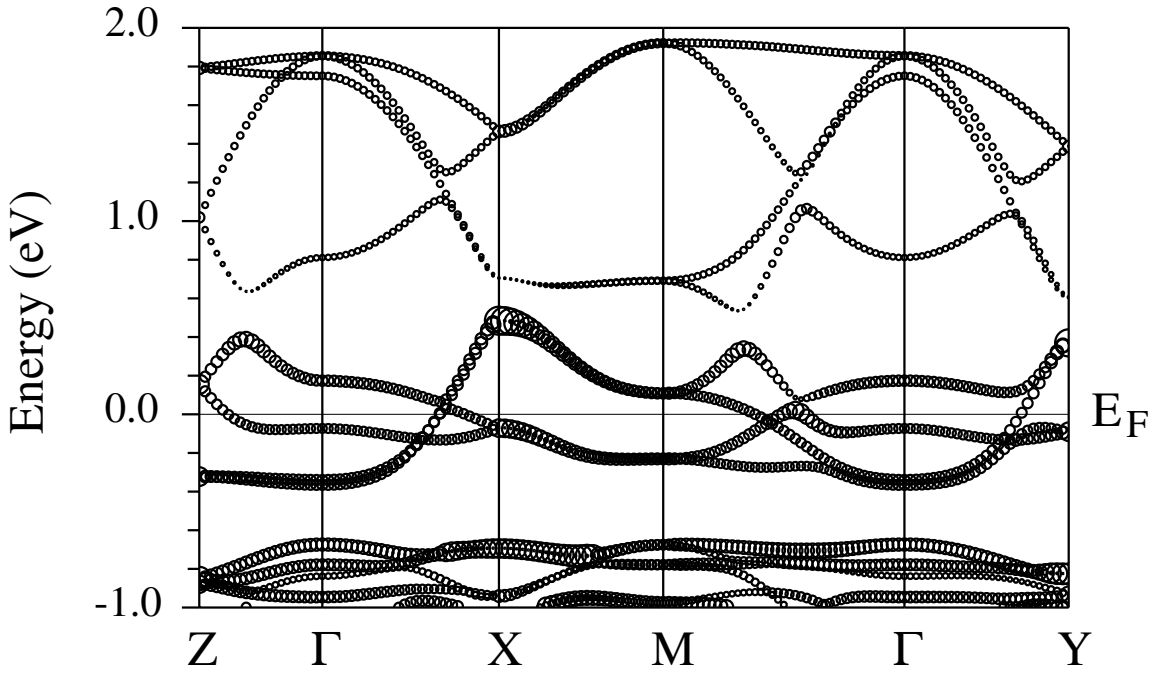

Monoclinic
(low-T)

DMFT calculations with realistic electronic structure for $LuNiO_3$

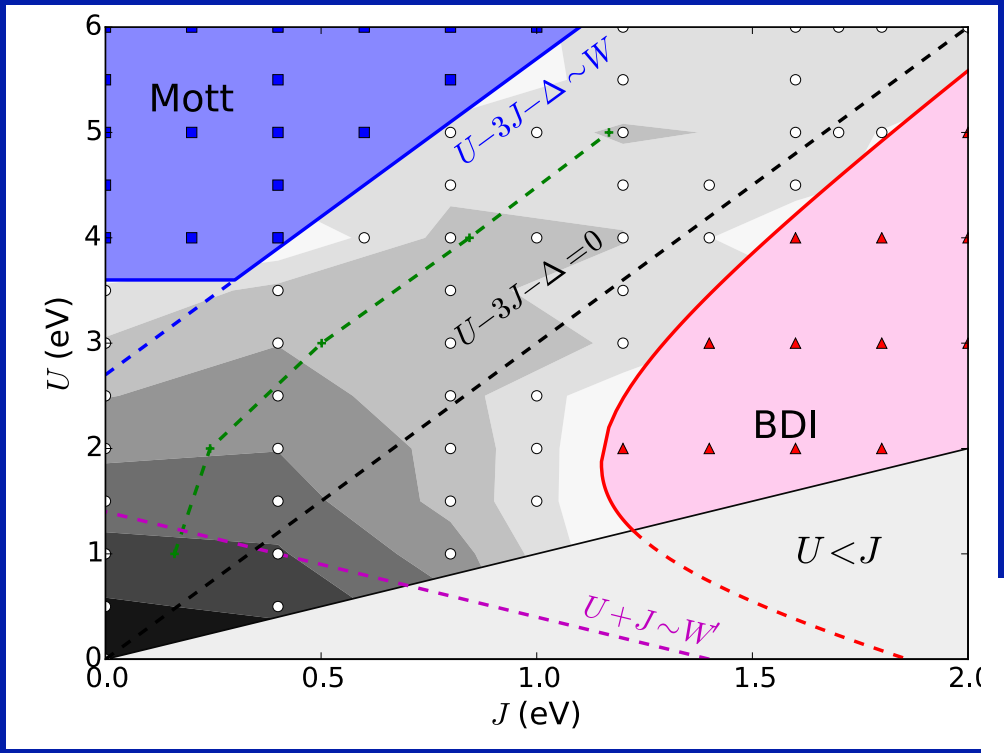

Orthorombic (hi-T)

Monoclinic (low-T)

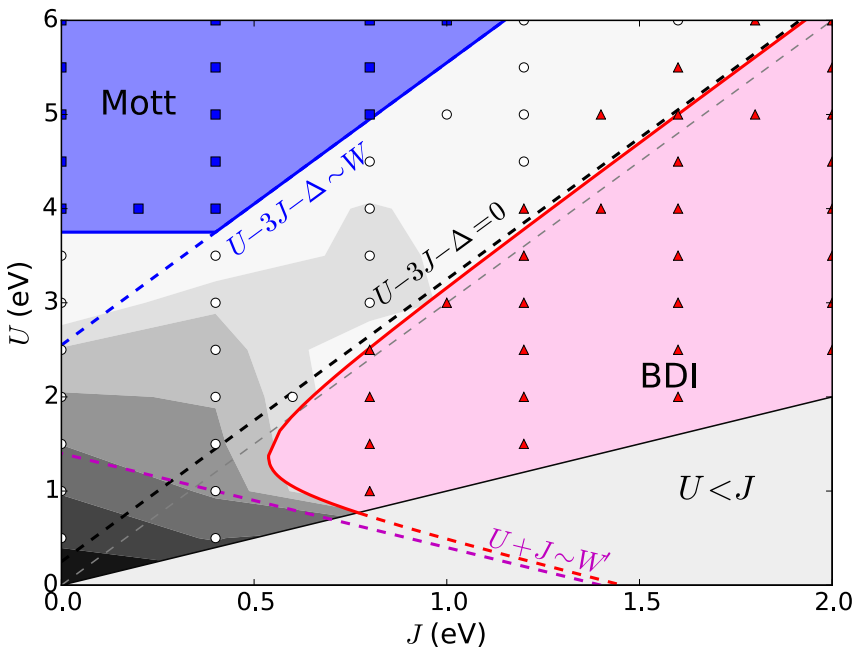

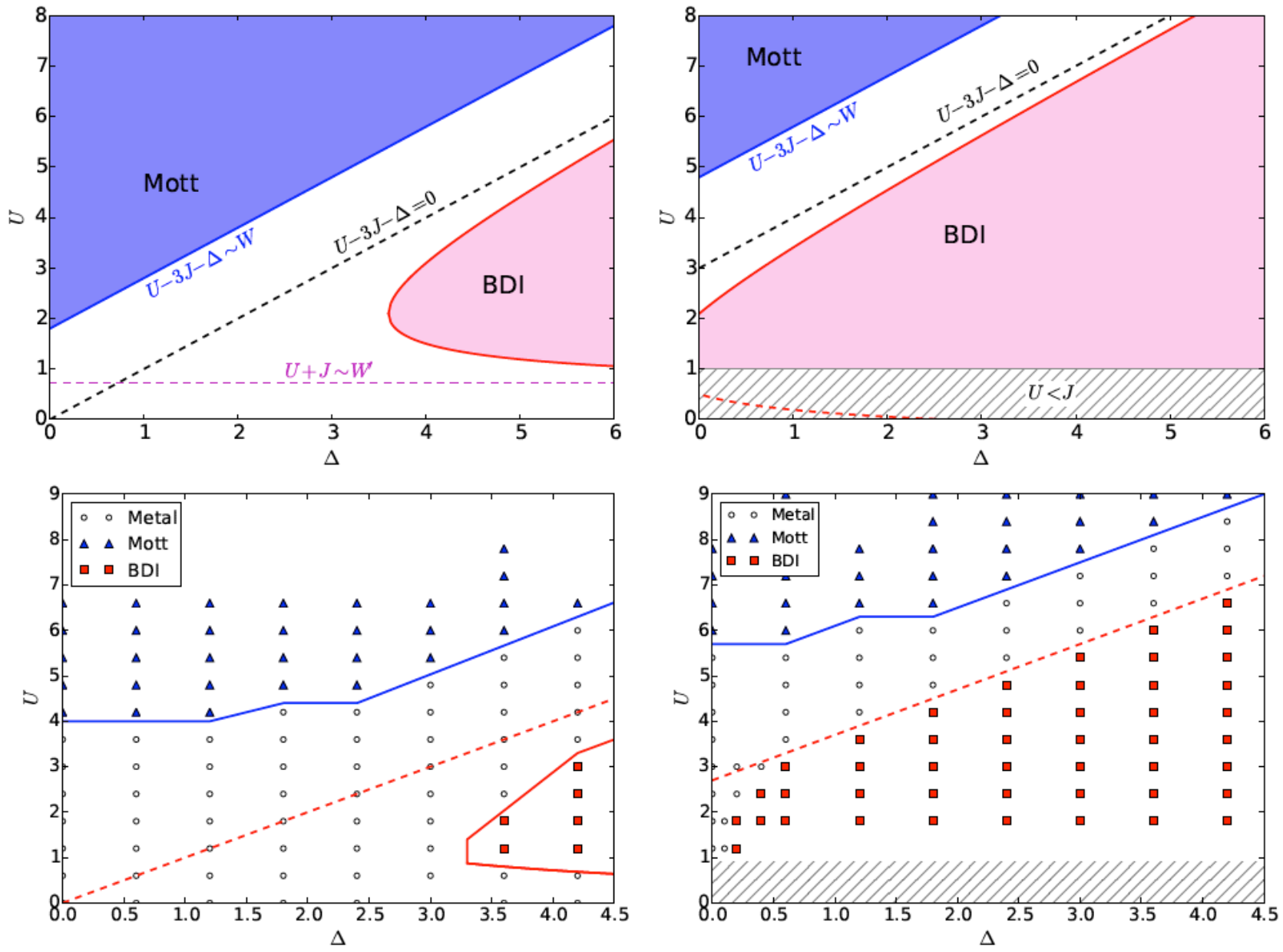

FIG. 5: Phase diagram of the two-orbital two-sublattice model. Top: Schematic phase diagrams based on qualitative considerations (see Appendix B) for $J < J_c$ (left) and $J > J_c$ (right). Bottom: Actual phase diagrams obtained from DMFT calculations on a Bethe lattice, for $J = 0.0$ (left), and $J = 0.9$ (right). The dashed red line corresponds to $U - 3J - \Delta = 0$. The phase boundaries are indicative, with actual data being represented by the markers.

Unfortunately, this idea does not fully work (yet)
for $LaNiO_3$ under
strain or simple heterostructures
… mostly because the infamous
Hund's coupling fights orbital polarization
(and importance of configuration $d^8\underline{L}$ Sawatzky)

See:
LDA+DMFT:
Han et al.
PRL 107, 206804 (2011
Peil, Ferrero & AG
PRB 2014
Experiments
@MPI-Stuttgart
Wu et al.
PRB 88, 125124 (2013)

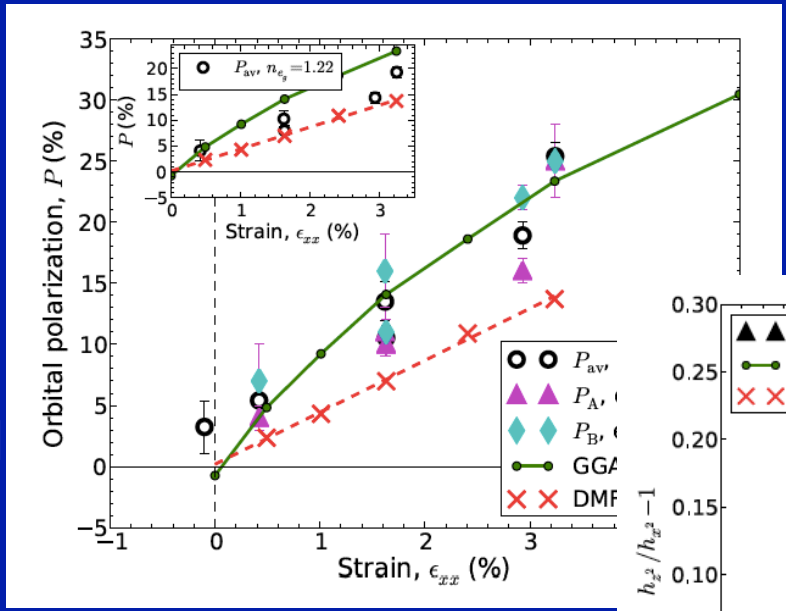

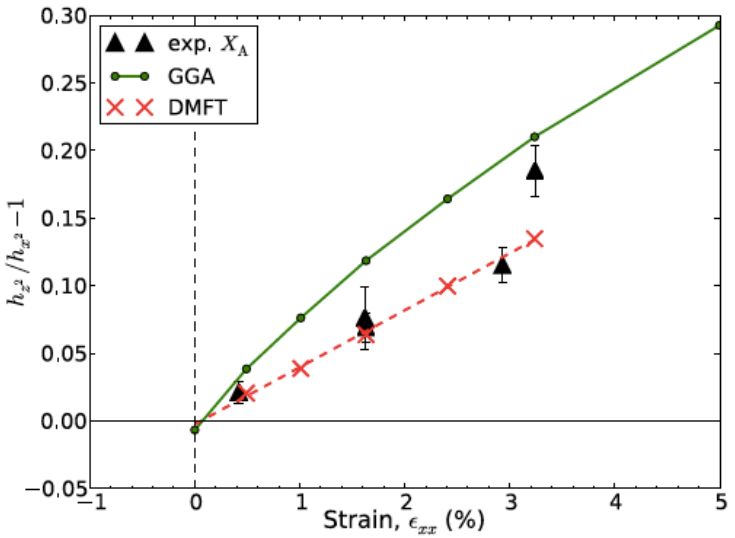

FIG. 12. (Color online) The ratio of the hole occupancies, X, as a function of strain (for experimental points the value for the inner layers, X_A, is used).

Still, `tricolor' heterostructures may work out

PRL **110,** 186402 (2013) PHYSICAL REVIEW LETTERS week ending 3 MAY 2013

Modifying the Electronic Orbitals of Nickelate Heterostructures via Structural Distortions

Hanghui Chen,[1,2,3] Divine P. Kumah,[3] Ankit S. Disa,[3] Frederick J. Walker,[3] Charles H. Ahn,[3,4] and Sohrab Ismail-Beigi[3]

[1]*Department of Physics, Columbia University, New York, New York 10027, USA*
[2]*Department of Applied Physics and Applied Mathematics, Columbia University, New York, New York 10027, USA*
[3]*Department of Applied Physics, Yale University, New Haven, Connecticut 06520, USA*
[4]*Department of Mechanical Engineering and Materials Science, Yale University, New Haven, Connecticut 06520, USA*

(Received 30 November 2012; revised manuscript received 15 February 2013; published 1 May 2013)

We describe a general materials design approach that produces large orbital energy splittings (orbital polarization) in nickelate heterostructures, creating a two-dimensional single-band electronic surface at the Fermi energy. The resulting electronic structure mimics that of the high temperature cuprate superconductors. The two key ingredients are (i) the construction of atomic-scale distortions about the Ni site via charge transfer and internal electric fields, and (ii) the use of three-component (tricomponent) superlattices to break inversion symmetry. We use *ab initio* calculations to implement the approach, with experimental verification of the critical structural motif that enables the design to succeed.

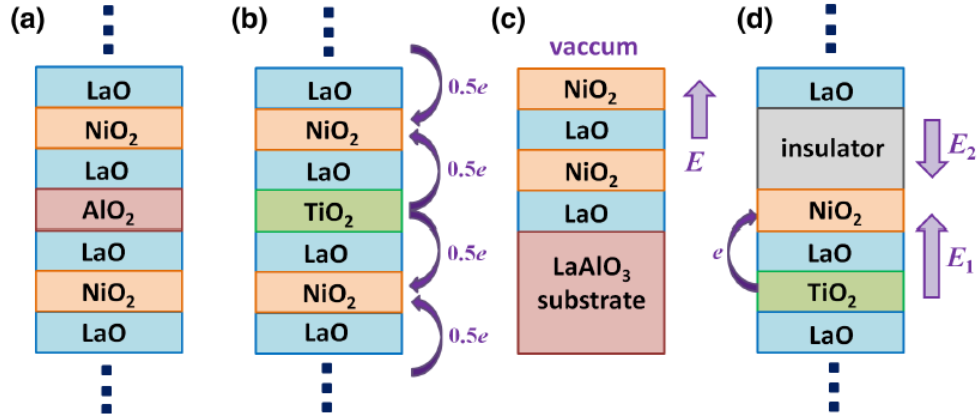

FIG. 1 (color online). Schematics of four nickelate heterostructures. (a) $(LaAlO_3)_1/(LaNiO_3)_1$ superlattice. (b) $(LaTiO_3)_1/(LaNiO_3)_1$ superlattice with nominal electron transfer from Ti to Ni. (c) NiO_2-terminated $LaNiO_3$ thin film on a $LaAlO_3$ substrate. (d) $(LaTiO_3)_1/(LaNiO_3)_1$/insulator superlattice with electron transfer and broken inversion symmetry. Arrows with "E" denote long-range electric fields in the material.